

博士論文

Theoretical Study of the Phase Transition and
Low-Temperature Property in Two-Dimensional
Coupled Antiferromagnets

二次元複合磁性体における
相転移と低温物性の理論的研究

伊藤 和博

広島大学大学院先端物質科学研究科

2016年3月

目次

1. 主論文

Theoretical Study of the Phase Transition and Low-Temperature Property in Two-Dimensional Coupled Antiferromagnets

(二次元複合磁性体における相転移と低温物性の理論的研究)

伊藤 和博

2. 公表論文

- (1) Mean Field Theory of a Coupled Heisenberg Model and Its Application to an Organic Antiferromagnet with Magnetic Anions

Kazuhiro Ito and Hiroshi Shimahara

Journal of the Physical Society of Japan, **85**, 024704-1 - 024704-7 (2016).

- (2) Stabilization of Long-Range Order by Additional Anisotropic Spins in Two-Dimensional Isotropic Heisenberg Antiferromagnets —A Possible Model of an Organic Compound with Magnetic Anions—

Hiroshi Shimahara and Kazuhiro Ito

Journal of the Physical Society of Japan, **83**, 114702-1 - 114702-7 (2014).

主論文

Acknowledgments

I would like to express my thanks to Professor Hiroshi Shimahara for his guidance and support throughout the course of my study. I am indebted to Professor Yutaka Nishio, Dr. Hiroshi Akiba, and Dr. Kazuo Shimada for useful discussions, information, and experimental data. I would also like to thank to Professor Katsuhiko Higuchi, Dr. Arata Tanaka, and Dr. Tatsuya Shishido for their encouragement.

Contents

1	Introduction	1
1.1	Background and purpose of the thesis	1
1.2	Stability of the antiferromagnetic order and dimensionality . .	7
1.2.1	Mermin–Wagner theorem	7
1.2.2	Spin wave theory	10
1.2.3	Tyablikov approximation	19
2	Theoretical Model for the Insulating Phase in λ-(BETS)₂FeCl₄	27
3	Analysis of the Low-Temperature Behavior	30
3.1	Low temperature limit	30
3.2	Mean-field theory	33
3.3	Results	38
3.3.1	Some typical cases	38
3.3.2	Reproduction of experimental results	39
3.4	Summary of the chapter	49
4	Phase Transition —Stabilization Mechanism of Antiferromagnetic Order—	52
4.1	Extension of the Tyablikov approximation	52
4.2	Results	58

4.3 Summary of the chapter	62
5 Conclusion	67

Chapter 1

Introduction

1.1 Background and purpose of the thesis

The two-dimensional organic conductor λ -(BETS)₂FeCl₄, where BETS stands for bis(ethylenedithio)tetraselenafulvalene, shows many intriguing properties [1–22], which originate from the magnetic anions FeCl₄ and the two-dimensionality of the conduction-electron system on BETS molecules. The system exhibits the antiferromagnetic insulating phase [1, 7, 23] at zero magnetic field and the magnetic-field-induced superconductivity [10, 24] at high fields, which may include the Fulde–Ferrell–Larkin–Ovchinnikov state [24–26]. The occurrence of the magnetic-field-induced superconductivity is explained by Jaccarino–Peter mechanism [27], in which the superconducting transition temperature is maximum when the effective Zeeman energy is zero. This suggests that conduction electrons are subject to the strong exchange field created by the 3d spins. Experimentally, the maximum transition temperature is 3 K at 33 T, i.e., $H_{c20}(3\text{ K}) = 33\text{ T}$, where $H_{c20}(T)$ is the pure orbital limit of the upper critical field in the absence of the Pauli paramagnetic pair-breaking effect. Such high pure-orbital limit means that the

interlayer hopping energy is very small in accordance with the presumption from the lattice structure.

The magnetic properties originate from two kinds of degrees of freedom, i.e., conduction π electrons in the BETS layers and localized 3d spins in the FeCl_4 anions. The five electrons in 3d orbitals of Fe^{3+} behave as a single localized spin with length $S = 5/2$ because they are in the high-spin state because of the strong Hund coupling. In the antiferromagnetic phase, π electrons are also considered to behave as localized spins with length $s = 1/2$ due to the strong correlation because the number of the π electrons per lattice site is equal to 1. Note that each pair of dimerized BETS molecules forms a lattice site. The strong electron correlation is supported by the fact that the transition temperature is high ($T_c \approx 8.3$ K) despite the absence of the Fermi-surface nesting. Furthermore, the metal-insulator transition was observed in the resistivity measurement [6]. The strong exchange fields created by the 3d spins may also favor the large spin moments of the π spins.

Just after the discovery of λ -(BETS) $_2$ FeCl $_4$, the antiferromagnetic long-range order was considered to be mainly formed by the 3d spins because of the large spin length. This picture was considered to be plausible because the antiferromagnetic order is formed by the 3d spins in the similar compounds κ -(BETS) $_2$ FeBr $_4$ [28–30] and κ -(BETS) $_2$ FeCl $_4$ [29, 30], which we call the κ systems hereafter. From the temperature dependence of the specific heat in these compounds, the sublattice magnetization in the 3d-spin system increases rapidly below the transition temperature. The phase diagrams for the κ systems, which include the antiferromagnetic phase at low fields and the field-induced superconducting phase at high fields [31], are explained by a unified model [32]. This model implies that the 3d spins play an indispensable role in forming the antiferromagnetic order.

Recently, it was found that roles of the π electrons and the 3d spins in λ -(BETS)₂FeCl₄ are different from those in the κ systems. The specific-heat measurement by Akiba et al. [17] revealed that the entropy of the 3d spins in λ -(BETS)₂FeCl₄ is consumed slowly when the temperature is lowered, in contrast to that in the κ systems. Thus, the 3d-spin system does not actively form the antiferromagnetic order but passively follows the antiferromagnetic order in the π -spin system. This picture is also supported by the experimental result of Mössbauer spectroscopy [33]. Therefore, the main interaction that sustains the antiferromagnetic order is the exchange interaction between the π spins. On the basis of these facts, the Schottky model [17] or paramagnetic model [33] has been studied. In this model, the 3d spins passively follow the constant exchange field Δ_d created by the π spins, as if they are free spins.

The Schottky model exhibits the six-level Schottky-type specific heat, which agrees well with the experimental data in λ -(BETS)₂FeCl₄ [18]. Some authors adopted this model [18, 22, 33], and reproduced not only the specific heat [18] but also the Mössbauer effect [33]. In the analysis of the specific heat by Akiba et al. [17], an additional scale factor is introduced to change the magnitude of specific heat. However, this factor causes a deviation of the total entropy from $Nk_B \ln(2S + 1)$, which directly follows from the fact that there are $(2S + 1)^N$ microscopic states, where N is the number of 3d spins. The derivation of the specific heat in the Schottky model is shown at the end of this chapter.

The Schottky model does not explain the stabilization mechanism of antiferromagnetic long-range order. The picture that the 3d spins passively follow the constant exchange field may give the idea that solely the π -spin system forms the antiferromagnetic order without the 3d-spin system. This presumption is incompatible with the experimental results for the sister com-

pound λ -(BETS) $_2$ GaCl $_4$ [1, 6, 18, 34], in which the π -spin system on BETS molecules does not exhibit the antiferromagnetic order. Therefore, the 3d spins are indispensable for the antiferromagnetic order, but the stabilization mechanism and the roles of the π and 3d spins are not described by the Schottky model.

The roles of the 3d spins are explained as follows: According to the Mermin–Wagner theorem, the isotropic low-dimensional system with short-range interactions does not undergo the magnetic transition at any finite temperature [35]. The low-dimensional thermal fluctuation suppresses the long-range order regardless the strength of the exchange interactions between the π spins are [12]. The anisotropy of the 3d spins and/or the interlayer interactions between BETS layers can stabilize the antiferromagnetic long-range order. In this thesis, we examine the stabilization mechanism by the anisotropy, which was addressed by Akiba et al. [17].

The anisotropy of λ -(BETS) $_2$ FeCl $_4$ has been studied in some experiments [11, 18, 23]. The magnetic susceptibility strongly depends on the direction of the magnetic fields [23]. From the result of the magnetic torque experiment, the angle between the magnetic easy axis and crystal c -axis is estimated to be $\theta \approx 30^\circ$ [11, 18, 36].

We assume a model based on the above argument. The absence of the antiferromagnetic order in λ -(BETS) $_2$ GaCl $_4$ indicates that the π -spin system on the BETS layers is isotropic in spin space. Thus, we adopt the two-dimensional isotropic antiferromagnetic Heisenberg model with $s = 1/2$ for π -electron system on BETS layers, which we call subsystem 1. In contrast, the 3d spins on the FeCl $_4$ anions are considered to have the uniaxial anisotropy. Thus, we adopt the anisotropic Heisenberg model with $S = 5/2$ to the 3d-spin system, which we call subsystem 2. In λ -(BETS) $_2$ FeCl $_4$, the

exchange interactions in subsystem 1 are stronger than those in subsystem 2, as mentioned above. The localized spin model that consists of subsystems 1 and 2 is called the coupled Heisenberg model, hereafter. The model is a possible minimum model that can describe the stabilization mechanism of the antiferromagnetic long-range order [37].

As a model of λ -(BETS)₂FeCl₄, the Kondo lattice model is more fundamental than the coupled Heisenberg model in a sense that π electrons are not assumed to be localized. Many authors have studied λ -(BETS)₂FeCl₄ in this model. Brossard et al. [7] studied the effect of the Ruderman–Kittel–Kasuya–Yosida (RKKY) interactions between 3d spins and the spin-flop transition in magnetic fields. Hotta and Fukuyama [38] obtained a unified phase diagram for the organic compounds including BETS molecules. They suggested that π electrons are localized in λ -(BETS)₂FeCl₄. C epas et al. [39] interpreted the magnetic field dependence of the electron state including the field-induced superconductivity. However, since these studies were carried out before the passive character of the 3d spins was revealed [17], this character was not taken into account.

As mentioned above, the coupled Heisenberg model is based on the localized spin picture of π electrons, which can be used only in the insulating phase of λ -(BETS)₂FeCl₄. The metal-insulator transition is explained in the Kondo lattice model, and the coupled Heisenberg model is derived from the Kondo lattice model in the insulating phase. However, we adopt the localized spin model as an effective model in the insulating phase from a phenomenological viewpoint.

For simplicity, we assume the square lattice. In the real material, the lattice structure and the configuration of the exchange interactions are more complex [12]. The triangular lattice may cause the geometrical frustration.

Because the antiferromagnetic order is stabilized in λ -(BETS) $_2$ FeCl $_4$, the imbalance of the coupling constants is considered to overcome the frustration effect from the phenomenological viewpoint. The difference in the spin-wave energy dispersion $\omega_{\mathbf{q}}$ does not change the qualitative result significantly because the behavior only near $\mathbf{q} = \mathbf{0}$ concerns for the stabilization of the long-range order.

In the analysis of the low temperature behaviors, we apply the mean-field approximation to the coupled Heisenberg model. We call the resultant model the mean-field model. The model is valid at low temperatures where the fluctuation is sufficiently small. Because the specific heat is reproduced very well by the Schottky model [17], the fluctuation is small at low temperatures. We reanalyze the experimental data using the least-squares method, and find the deviation from the Schottky model, where we check the validity of the mean-field approximation and the localized spin picture. We estimate the model parameters and confirm that the condition $J_{12}, J_2 \ll J_1$ is satisfied. We also reveal some properties of the magnetic anisotropy.

For the study of the phase transition, we extend the Green function theory called the Tyablikov approximation [40]. The two subsystems are different in the spin length and the anisotropy in the spin space. Therefore, they fluctuate in the quite different spatial and temporal scales. Since the 3d spins fluctuate more slowly than the π spins, we adopt the mean-field approximation for the 3d spins. In this approximation, the transition temperature tends to be higher than the true value. In spite of this tendency, it is non-trivial whether the experimental transition temperature is reproduced by this model because the mean-field transition temperature of the independent 3d-spin subsystem is much smaller than the experimental value. The treatment for the π -spin subsystem needs to be consistent with Mermin–Wagner theorem [35]. Thus,

we apply the Tyablikov approximation to the π spins. In this approximation, the isolated π -spin system does not exhibit the antiferromagnetic long-range order at any finite temperature.

We summarize the outline of the thesis. In Chap. 1.2, we review the spin wave theory and the Tyablikov approximation for the ferromagnetic and antiferromagnetic Heisenberg models. In Chap. 2, the coupled Heisenberg model is presented. In Chap. 3, we adopt the mean-field approximation for the coupled Heisenberg model at low temperatures, and analyze the experimental data of the specific heat and the spin susceptibility in λ -(BETS) $_2$ FeCl $_4$. In Chap. 4 we examine the coupled Heisenberg model on the basis of the Tyablikov approximation, and calculate the critical temperature and the sublattice magnetizations. In Chap. 5, the conclusion of this thesis is presented. We use units in which $\hbar = 1$ and $k_B = 1$, and define $\beta \equiv 1/k_B T$.

1.2 Stability of the antiferromagnetic order and dimensionality

1.2.1 Mermin–Wagner theorem

In this section, we shall review the Mermin–Wagner theorem, which shows that the isotropic Heisenberg model with short-range interactions does not exhibit the ferromagnetic or antiferromagnetic long-range order at any finite temperature.

We examine the Heisenberg model

$$H = - \sum_{RR'} J_{R-R'} \mathbf{S}_R \cdot \mathbf{S}_{R'} - h \sum_R S_R^z e^{i\mathbf{K} \cdot \mathbf{R}}. \quad (1.1)$$

We assume that $J_0 = 0$ and $J_{\mathbf{R}} = J_{-\mathbf{R}}$.

We define

$$\mathbf{S}_{\mathbf{k}} \equiv \sum_{\mathbf{R}} e^{-i\mathbf{k}\cdot\mathbf{R}} \mathbf{S}_{\mathbf{R}}, \quad (1.2)$$

$$J_{\mathbf{k}} \equiv \sum_{\mathbf{R}} e^{-i\mathbf{k}\cdot\mathbf{R}} J_{\mathbf{R}}. \quad (1.3)$$

Thus, we obtain

$$\mathbf{S}_{\mathbf{R}} = \frac{1}{N} \sum_{\mathbf{k}} e^{i\mathbf{k}\cdot\mathbf{R}} \mathbf{S}_{\mathbf{k}}, \quad (1.4)$$

$$J_{\mathbf{R}} = \frac{1}{N} \sum_{\mathbf{k}} e^{i\mathbf{k}\cdot\mathbf{R}} J_{\mathbf{k}}, \quad (1.5)$$

where N is the number of the sites and the summation $\sum_{\mathbf{k}}$ is taken over the 1st Brillouin zone.

The Bogoliubov's inequality is

$$\frac{1}{2} \langle \{A, A^\dagger\} \rangle \langle [[C, H], C^\dagger] \rangle \geq k_{\text{B}} T |\langle [C, A] \rangle|^2 \quad (1.6)$$

for any operators A , B , and C , where H is the Hamiltonian, and $\langle \dots \rangle$ denotes the thermal average. Thus, we obtain

$$\frac{1}{2} \langle \{A, A^\dagger\} \rangle \geq k_{\text{B}} T \frac{|\langle [C, A] \rangle|^2}{\langle [[C, H], C^\dagger] \rangle} \geq 0. \quad (1.7)$$

When $A = S_{-\mathbf{k}-\mathbf{K}}^-$, $C = S_{\mathbf{k}}^+$, we obtain

$$\frac{1}{2} \sum_{\mathbf{k}} \langle \{S_{-\mathbf{k}-\mathbf{K}}^-, (S_{-\mathbf{k}-\mathbf{K}}^-)^\dagger\} \rangle \geq k_{\text{B}} T \sum_{\mathbf{k}} \frac{|\langle [S_{\mathbf{k}}^+, S_{-\mathbf{k}-\mathbf{K}}^-] \rangle|^2}{\langle [[S_{\mathbf{k}}^+, H], (S_{\mathbf{K}}^+)^\dagger] \rangle} \geq 0. \quad (1.8)$$

We also find that

$$\langle \{S_{-\mathbf{k}-\mathbf{K}}^-, (S_{-\mathbf{k}-\mathbf{K}}^-)^\dagger\} \rangle < 2N^2 S(S+1), \quad (1.9)$$

$$|\langle [S_{\mathbf{k}}^+, S_{-\mathbf{k}-\mathbf{K}}^-] \rangle|^2 = 4N^2 M^2, \quad (1.10)$$

$$\langle [[S_{\mathbf{k}}^+, H], (S_{\mathbf{K}}^+)^\dagger] \rangle < 2N \left(2S(S+1)k^2 \sum_{\mathbf{R}} R^2 |J_{\mathbf{R}}| + |hM| \right), \quad (1.11)$$

where we define

$$M \equiv \frac{1}{N} \sum_{\mathbf{R}} e^{i\mathbf{K}\cdot\mathbf{R}} \langle S_{\mathbf{R}}^z \rangle. \quad (1.12)$$

Therefore, we obtain

$$\begin{aligned} S(S+1) &> \frac{2k_{\text{B}}TM^2}{N} \sum_{\mathbf{k}} \frac{1}{\alpha k^2 + \gamma} \\ &= \frac{2k_{\text{B}}TM^2}{v} \int \frac{d^d k}{(2\pi)^d} \frac{1}{\alpha k^2 + \gamma} \end{aligned} \quad (1.13)$$

for d -dimensional systems, where the integral is taken over the 1st Brillouin zone. α and γ are defined as

$$\alpha \equiv 2S(S+1) \sum_{\mathbf{R}} |J_{\mathbf{R}}| R^2, \quad (1.14)$$

$$\gamma \equiv |hM|. \quad (1.15)$$

v denotes the volume of the unit cell.

In the case of one-dimensional systems, we find

$$\int \frac{dk}{2\pi} \frac{1}{\alpha k^2 + \gamma} > \int_{-k_0}^{k_0} \frac{dk}{2\pi} \frac{1}{\alpha k^2 + \gamma} = \frac{1}{\pi\sqrt{\alpha\gamma}} \arctan \left(\sqrt{\frac{\alpha}{\gamma}} k_0 \right). \quad (1.16)$$

Thus, we obtain

$$|M|^3 < |h|\omega \left[\frac{\pi v S(S+1)}{2k_B T k_0 \arctan\left(\sqrt{\omega/|Mh|}\right)} \right]^2 \quad (1.17)$$

with $\omega \equiv \alpha k_0^2$. We find that M becomes zero when h vanishes, which implies the absence of the ferromagnetic or antiferromagnetic long-range order in the one-dimensional isotropic spin system at any finite temperature.

In the case of two-dimensional systems, we find

$$\begin{aligned} \int \frac{dk}{2\pi} \frac{1}{\alpha k^2 + \gamma} &> \frac{1}{(2\pi)^2} \int_0^{k_0} dk \int_0^{2\pi} d\theta \frac{1}{\alpha k^2 + \gamma} \\ &= \frac{1}{4\pi\alpha} \ln\left(\frac{\alpha}{\gamma} k_0^2 + 1\right). \end{aligned} \quad (1.18)$$

Thus, we obtain

$$M^2 < \frac{2\pi v S(S+1)}{k_0^2} \frac{\omega/k_B T}{\ln(1 + \omega/|Mh|)}. \quad (1.19)$$

Therefore, we also find that M becomes zero when h vanishes, which implies the absence of the ferromagnetic or antiferromagnetic long-range order in the one-dimensional isotropic spin system at any finite temperature.

1.2.2 Spin wave theory

In this section, we review the spin wave theory for the ferromagnetic and antiferromagnetic Heisenberg models. We use the Holstein-Primakoff transformation, which rewrites the spin operators in terms of the creation and annihilation operators of bosons. The Bose excitations correspond to the fluctuations of the spins. At sufficiently low temperatures, the Hamiltonian is approximately expressed as that of the free boson system because the num-

ber of bosons is small. We derive the expressions of the dispersion relation of the bosons, the magnetization, the internal energy, and the specific heat.

The ferromagnetic case

We briefly review the ferromagnetic case. The Hamiltonian of the ferromagnetic Heisenberg model is

$$H = -J \sum_{\langle i,j \rangle} \mathbf{S}_i \cdot \mathbf{S}_j, \quad (1.20)$$

where $J > 0$. The Holstein-Primakoff transformation is defined as

$$S_i^z = S - a_i^\dagger a_i, \quad (1.21)$$

$$S_i^+ = \sqrt{2S} \sqrt{1 - \frac{a_i^\dagger a_i}{2S}} a_i, \quad (1.22)$$

$$S_i^- = \sqrt{2S} a_i^\dagger \sqrt{1 - \frac{a_i^\dagger a_i}{2S}}, \quad (1.23)$$

where a_i^\dagger and a_i are the creation and annihilation operators of bosons, respectively, which satisfy the commutation relations as $[a_i, a_{i'}^\dagger] = \delta_{ii'}$ and $[a_i^\dagger, a_{i'}^\dagger] = [a_i, a_{i'}] = 0$. The eigenvalue m_i of S_i^z in Eq. (1.21) takes not only $m_i = -S, -S + 1, \dots, S$, but also $-S - 1, -S - 2, \dots, -\infty$ due to the property of the number operator $\hat{n}_i \equiv a_i^\dagger a_i$. We refer to the eigenstate of S_i^z that belongs to the eigenvalue m_i as $|m_i\rangle$.

At sufficiently low temperatures, the spin deviation is sufficiently small, i.e., $\langle a_i^\dagger a_i \rangle / S \ll 1$. Thus, we expand the Holstein-Primakoff transformation

given in Eqs. (1.22) and (1.23) with respect to $a_i^\dagger a_i$ and find

$$S_i^+ \simeq \sqrt{2S} \left(a_i - \frac{1}{4S} a_i^\dagger a_i a_i \right), \quad (1.24)$$

$$S_i^- \simeq \sqrt{2S} \left(a_i^\dagger - \frac{1}{4S} a_i^\dagger a_i^\dagger a_i \right), \quad (1.25)$$

where a_i^\dagger and a_i are the creation and annihilation operators of the boson at site i , respectively. We define

$$a_{\mathbf{k}} \equiv \frac{1}{\sqrt{N}} \sum_i e^{-i\mathbf{k}\cdot\mathbf{R}_i} a_i, \quad (1.26)$$

$$a_{\mathbf{k}}^\dagger \equiv \frac{1}{\sqrt{N}} \sum_i e^{i\mathbf{k}\cdot\mathbf{R}_i} a_i^\dagger, \quad (1.27)$$

where \mathbf{R}_i is the position vector of site i . Thus, the inverse transformations are

$$a_i = \frac{1}{\sqrt{N}} \sum_{\mathbf{k}} e^{i\mathbf{k}\cdot\mathbf{R}_i} a_{\mathbf{k}}, \quad (1.28)$$

$$a_i^\dagger = \frac{1}{\sqrt{N}} \sum_{\mathbf{k}} e^{-i\mathbf{k}\cdot\mathbf{R}_i} a_{\mathbf{k}}^\dagger. \quad (1.29)$$

Therefore, we obtain

$$S_i^+ \simeq \sqrt{\frac{2S}{N}} \left(\sum_{\mathbf{k}} e^{i\mathbf{k}\cdot\mathbf{R}_i} a_{\mathbf{k}} - \frac{1}{4NS} \sum_{\mathbf{k}\mathbf{k}'\mathbf{k}''} e^{i(-\mathbf{k}+\mathbf{k}'+\mathbf{k}'')\cdot\mathbf{R}_i} a_{\mathbf{k}}^\dagger a_{\mathbf{k}'} a_{\mathbf{k}''} \right), \quad (1.30)$$

$$S_i^- \simeq \sqrt{\frac{2S}{N}} \left(\sum_{\mathbf{k}} e^{-i\mathbf{k}\cdot\mathbf{R}_i} a_{\mathbf{k}}^\dagger - \frac{1}{4NS} \sum_{\mathbf{k}\mathbf{k}'\mathbf{k}''} e^{i(-\mathbf{k}-\mathbf{k}'+\mathbf{k}'')\cdot\mathbf{R}_i} a_{\mathbf{k}}^\dagger a_{\mathbf{k}'}^\dagger a_{\mathbf{k}''} \right), \quad (1.31)$$

$$S_i^z = S - \frac{1}{N} \sum_{\mathbf{k}\mathbf{k}'} e^{i(\mathbf{k}'-\mathbf{k})\cdot\mathbf{R}_i} a_{\mathbf{k}}^\dagger a_{\mathbf{k}'}. \quad (1.32)$$

From Eqs. (1.30)–(1.32), the Hamiltonian is rewritten as

$$H \simeq \sum_{\mathbf{k}} \omega_{\mathbf{k}} \hat{n}_{\mathbf{k}} - NzJS^2 \quad (1.33)$$

with

$$\omega_{\mathbf{k}} \equiv zJS(1 - \gamma_{\mathbf{k}}), \quad (1.34)$$

$$\gamma_{\mathbf{k}} \equiv \frac{1}{z} \sum_{\boldsymbol{\rho}} e^{i\mathbf{k}\cdot\boldsymbol{\rho}}, \quad (1.35)$$

where z is the number of the nearest neighbor sites, $\hat{n}_{\mathbf{k}} \equiv a_{\mathbf{k}}^\dagger a_{\mathbf{k}}$, and $\boldsymbol{\rho}$ are the vectors connecting the nearest neighbor sites.

At sufficiently low temperatures, the low-energy excitations play an important role in the property of the system. By using $\gamma_{\mathbf{k}} \simeq 1 - Dk^2$ for small $k \equiv |\mathbf{k}|$, the dispersion relation of those excitations is approximately written as

$$\omega_{\mathbf{k}} \simeq zJSDk^2 \equiv ak^2, \quad (1.36)$$

where D is a constant which depends on the crystal structure. Omitting the constant term of Eq. (1.33), we obtain

$$H \simeq \sum_{\mathbf{k}} \omega_{\mathbf{k}} \hat{n}_{\mathbf{k}}. \quad (1.37)$$

Thus, in three dimensional systems, the magnetization M is expressed as

$$M \equiv \frac{1}{N} \sum_i \langle S_i^z \rangle = S - \frac{\zeta(3/2)}{8\pi^{3/2}} \frac{V}{N} a^{-3/2} T^{3/2} \quad (1.38)$$

where $\zeta(x)$ is the Riemann zeta function, $\zeta(3/2) \simeq 2.612$, and V is the volume

of the system. The internal energy U and specific heat C are written as

$$U \equiv \langle H \rangle = \frac{3\zeta(5/2)}{16\pi^{3/2}} V a^{-3/2} T^{5/2}, \quad (1.39)$$

$$C \equiv \frac{\partial U}{\partial T} = \frac{15\zeta(5/2)}{32\pi^{3/2}} V a^{-3/2} T^{3/2}, \quad (1.40)$$

where $\zeta(5/2) \simeq 1.342$.

The antiferromagnetic case

Next, we review the antiferromagnetic case. The Hamiltonian of the antiferromagnetic Heisenberg model is

$$H = J \sum_{(i,j)} \mathbf{S}_i \cdot \mathbf{S}_j, \quad (1.41)$$

where $J > 0$.

We divide the lattice into sublattices A and B . Similarly to the ferromagnetic case, the Holstein-Primakoff transformation is defined as

$$S_l^z = S - a_l^\dagger a_l, \quad (1.42)$$

$$S_l^+ = \sqrt{2S} \sqrt{1 - \frac{a_l^\dagger a_l}{2S}} a_l, \quad (1.43)$$

$$S_l^- = \sqrt{2S} a_l^\dagger \sqrt{1 - \frac{a_l^\dagger a_l}{2S}} \quad (1.44)$$

for $l \in A$,

$$S_m^z = -S + b_m^\dagger b_m, \quad (1.45)$$

$$S_m^+ = \sqrt{2S} b_m^\dagger \sqrt{1 - \frac{b_m^\dagger b_m}{2S}}, \quad (1.46)$$

$$S_m^- = \sqrt{2S} \sqrt{1 - \frac{b_m^\dagger b_m}{2S}} b_m \quad (1.47)$$

for $m \in B$, where a_l^\dagger , a_l , b_m^\dagger , and b_m are the creation and annihilation operators of bosons, which satisfy the commutation relations of bosons, $[a_l, a_{l'}^\dagger] = \delta_{ll'}$, $[b_m, b_{m'}^\dagger] = \delta_{mm'}$, and $[a_l^\dagger, a_{l'}^\dagger] = [a_l, a_{l'}] = [b_m^\dagger, b_{m'}^\dagger] = [b_m, b_{m'}] = 0$, and the orthogonality condition $[a_l, b_m^\dagger] = [a_l^\dagger, b_m] = 0$.

At sufficiently low temperatures, the spin deviations are sufficiently small, i.e., $\langle a_l^\dagger a_l \rangle / S \ll 1$, and $\langle b_m^\dagger b_m \rangle / S \ll 1$. Thus, the Holstein-Primakoff transformations given in Eqs. (1.42)–(1.47) are approximately written as

$$S_l^+ \simeq \sqrt{2S} \left(a_l - \frac{a_l^\dagger a_l a_l}{4S} \right), \quad (1.48)$$

$$S_l^- \simeq \sqrt{2S} \left(a_l^\dagger - \frac{a_l^\dagger a_l^\dagger a_l}{4S} \right), \quad (1.49)$$

for $l \in A$,

$$S_m^+ \simeq \sqrt{2S} \left(b_m^\dagger - \frac{b_m^\dagger b_m^\dagger b_m}{4S} \right), \quad (1.50)$$

$$S_m^- \simeq \sqrt{2S} \left(b_m - \frac{b_m^\dagger b_m b_m}{4S} \right), \quad (1.51)$$

for $m \in B$. When only the 1st terms in Eqs. (1.48)–(1.51) are retained, we

find

$$\mathbf{S}_l \cdot \mathbf{S}_m \simeq -S^2 + S(a_l^\dagger a_l + a_l^\dagger b_m^\dagger + a_l b_m + b_m^\dagger b_m). \quad (1.52)$$

We define the transformation as

$$a_{\mathbf{k}} \equiv \sqrt{\frac{2}{N}} \sum_l' e^{-i\mathbf{k} \cdot \mathbf{R}_l} a_l, \quad (1.53)$$

$$a_{\mathbf{k}}^\dagger = \sqrt{\frac{2}{N}} \sum_l' e^{i\mathbf{k} \cdot \mathbf{R}_l} a_l^\dagger, \quad (1.54)$$

$$b_{\mathbf{k}} \equiv \sqrt{\frac{2}{N}} \sum_m' e^{-i\mathbf{k} \cdot \mathbf{R}_m} b_l, \quad (1.55)$$

$$b_{\mathbf{k}}^\dagger = \sqrt{\frac{2}{N}} \sum_m' e^{i\mathbf{k} \cdot \mathbf{R}_m} b_l^\dagger, \quad (1.56)$$

where the sums \sum_l' and \sum_m' are taken over all sites of sublattices A and B , respectively. \mathbf{R}_l and \mathbf{R}_m are the position vectors of site l in sublattice A and site m in sublattice B , respectively. Thus, the inverse transformations are

$$a_l = \sqrt{\frac{2}{N}} \sum_{\mathbf{k}}' e^{i\mathbf{k} \cdot \mathbf{R}_l} a_{\mathbf{k}}, \quad (1.57)$$

$$a_l^\dagger = \sqrt{\frac{2}{N}} \sum_{\mathbf{k}}' e^{-i\mathbf{k} \cdot \mathbf{R}_l} a_{\mathbf{k}}^\dagger, \quad (1.58)$$

$$b_m = \sqrt{\frac{2}{N}} \sum_{\mathbf{k}}' e^{i\mathbf{k} \cdot \mathbf{R}_m} b_{\mathbf{k}}, \quad (1.59)$$

$$b_m^\dagger = \sqrt{\frac{2}{N}} \sum_{\mathbf{k}}' e^{-i\mathbf{k} \cdot \mathbf{R}_m} b_{\mathbf{k}}^\dagger, \quad (1.60)$$

where the sum $\sum_{\mathbf{k}}'$ is taken over \mathbf{k} in the 1st Brillouin zone in the antiferro-

magnetic phase. Therefore, we find

$$H \simeq zJS \sum_{\mathbf{k}}' (a_{\mathbf{k}}^\dagger a_{\mathbf{k}} + \gamma_{-\mathbf{k}} a_{\mathbf{k}}^\dagger b_{-\mathbf{k}}^\dagger + \gamma_{\mathbf{k}} a_{\mathbf{k}} a_{\mathbf{k}} + b_{-\mathbf{k}} b_{-\mathbf{k}}^\dagger) - \frac{1}{2} NzJS(S+1) \quad (1.61)$$

with

$$\gamma_{\mathbf{k}} \equiv \frac{1}{z} \sum_{\rho} e^{i\mathbf{k}\cdot\rho}. \quad (1.62)$$

The Bogoliubov transformation is defined as

$$\begin{pmatrix} \alpha_{\mathbf{k}} \\ \beta_{-\mathbf{k}}^\dagger \end{pmatrix} \equiv \begin{pmatrix} u_{\mathbf{k}} & v_{\mathbf{k}} \\ v_{\mathbf{k}} & u_{\mathbf{k}} \end{pmatrix} \begin{pmatrix} a_{\mathbf{k}} \\ b_{-\mathbf{k}}^\dagger \end{pmatrix}, \quad (1.63)$$

where $u_{\mathbf{k}}^2 - v_{\mathbf{k}}^2 = 1$, and $u_{\mathbf{k}}$ and $v_{\mathbf{k}}$ are real. $\alpha_{\mathbf{k}}$ and $\beta_{\mathbf{k}}$ satisfy the commutation relations of bosons $[\alpha_{\mathbf{k}}, \alpha_{\mathbf{k}'}^\dagger] = [\beta_{\mathbf{k}}, \beta_{\mathbf{k}'}^\dagger] = \delta_{\mathbf{k}\mathbf{k}'}$, $[\alpha_{\mathbf{k}}, \alpha_{\mathbf{k}'}] = [\alpha_{\mathbf{k}}^\dagger, \alpha_{\mathbf{k}'}^\dagger] = [\beta_{\mathbf{k}}, \beta_{\mathbf{k}'}] = [\beta_{\mathbf{k}}^\dagger, \beta_{\mathbf{k}'}^\dagger] = 0$, and the orthogonality condition $[\alpha_{\mathbf{k}}, \beta_{\mathbf{k}'}^\dagger] = [\alpha_{\mathbf{k}}^\dagger, \beta_{\mathbf{k}'}^\dagger] = 0$. To diagonalize the Hamiltonian given in Eq. (1.61), we choose $u_{\mathbf{k}}$ and $v_{\mathbf{k}}$ as

$$u_{\mathbf{k}} = \frac{1}{\sqrt{2}} \left(\frac{1}{\sqrt{1 - \gamma_{\mathbf{k}}^2}} + 1 \right)^{1/2}, \quad (1.64)$$

$$v_{\mathbf{k}} = \frac{1}{\sqrt{2}} \left(\frac{1}{\sqrt{1 - \gamma_{\mathbf{k}}^2}} - 1 \right)^{1/2}. \quad (1.65)$$

Therefore, we obtain

$$H \simeq \sum_{\mathbf{k}}' \omega_{\mathbf{k}} (\alpha_{\mathbf{k}}^\dagger \alpha_{\mathbf{k}} + \beta_{\mathbf{k}}^\dagger \beta_{\mathbf{k}}) + E_0, \quad (1.66)$$

where

$$E_0 = \sum_{\mathbf{k}}' \omega_{\mathbf{k}} - \frac{1}{2} N z J S (S + 1), \quad (1.67)$$

$$\omega_{\mathbf{k}} = z J S \sqrt{1 - \gamma_{\mathbf{k}}^2}. \quad (1.68)$$

At sufficiently low temperatures, using $\gamma_{\mathbf{k}} \simeq 1 - Dk^2$, we find

$$\omega_{\mathbf{k}} \simeq z J S \sqrt{D} k \equiv a k. \quad (1.69)$$

Thus, in the three-dimensional system, the sublattice magnetization M is obtained as

$$\begin{aligned} M &\equiv \frac{2}{N} \sum_l' \langle S_l^z \rangle = -\frac{2}{N} \sum_m' \langle S_m^z \rangle \\ &= S - \frac{2}{N} \sum_{\mathbf{k}}' \frac{1}{\sqrt{1 - \gamma_{\mathbf{k}}^2}} \frac{1}{e^{\beta \omega_{\mathbf{k}}} - 1} - \frac{1}{N} \sum_{\mathbf{k}}' \left(\frac{1}{\sqrt{1 - \gamma_{\mathbf{k}}^2}} - 1 \right) \\ &= S - \Delta S - \frac{1}{6a^2 \sqrt{D}} \frac{V}{N} T^2 \end{aligned} \quad (1.70)$$

for $l \in A$ and $m \in B$, where ΔS is the shrinkage of spin expectation value at $T = 0$, which is expressed as

$$\Delta S = \frac{1}{N} \sum_{\mathbf{k}}' \left(\frac{1}{\sqrt{1 - \gamma_{\mathbf{k}}^2}} - 1 \right). \quad (1.71)$$

The internal energy U and the specific heat C are written as

$$U \equiv \langle H \rangle = E_0 + \frac{\pi^2}{15} V a^{-3} T^4, \quad (1.72)$$

$$C \equiv \frac{\partial U}{\partial T} = \frac{4\pi^2}{15} V a^{-3} T^3. \quad (1.73)$$

1.2.3 Tyablikov approximation

In this section, we explain the Tyablikov approximation for the ferromagnetic and antiferromagnetic Heisenberg models. This method is a decoupling method for the Green function, in which the fluctuation effect is incorporated. We derive the expression for the Green function by solving the equation of motion. From the Green function, we derive the self-consistent equation for the magnetization or the sublattice magnetization, and obtain the expression of the critical temperature. We show that the one- and two-dimensional systems do not exhibit the long-range order at any finite transition temperatures. This result agrees with the Mermin–Wagner theorem.

The ferromagnetic case

We examine the ferromagnetic Heisenberg model

$$H = -J \sum_{(i,j)} \mathbf{S}_i \cdot \mathbf{S}_j \quad (1.74)$$

with the coupling constant $J > 0$ and the spin at site i , $\mathbf{S}_i = (S_i^x, S_i^y, S_i^z)$, where the sum $\sum_{(i,j)}$ is taken over all pairs of the nearest neighbor sites.

Let us derive the expression for the Green function. We consider the retarded Green function

$$G_{ij}(t) \equiv \langle S_i^+ | S_j^- \rangle, \quad (1.75)$$

where $S_i^\pm \equiv S_i^x \pm iS_i^y$, $\langle A | B \rangle \equiv -i\theta(t)\langle [A(t), B] \rangle$, and $A(t) \equiv e^{iHt} A e^{-iHt}$.

In the equation of motion for the retarded Green function

$$i \frac{\partial}{\partial t} \langle A | B \rangle = \delta(t) \langle [A, B] \rangle + i\theta(t) \langle [[H, A(t)], B] \rangle, \quad (1.76)$$

setting $A = S_i^+$ and $B = S_j^-$, we obtain

$$i\frac{\partial}{\partial t}G_{ij}(t) = 2\langle S_i^z \rangle \delta_{ij} \delta(t) + J \sum_{\boldsymbol{\rho}} \langle (S_{i+\boldsymbol{\rho}}^z S_i^+ - S_i^z S_{i+\boldsymbol{\rho}}^+) | S_j^- \rangle, \quad (1.77)$$

where the site index $i + \boldsymbol{\rho}$ means the nearest neighbor site of the site i in the direction of $\boldsymbol{\rho}$. Adopting the Tyablikov approximation

$$\langle S_{i+\boldsymbol{\rho}}^z S_i^+ | S_j^- \rangle \simeq \langle S_{i+\boldsymbol{\rho}}^z \rangle \langle S_i^+ | S_j^- \rangle, \quad (1.78)$$

$$\langle S_i^z S_{i+\boldsymbol{\rho}}^+ | S_j^- \rangle \simeq \langle S_i^z \rangle \langle S_{i+\boldsymbol{\rho}}^+ | S_j^- \rangle, \quad (1.79)$$

we obtain

$$i\frac{\partial}{\partial t}G_{ij}(t) = 2M\delta_{ij}\delta(t) + zJM \left\{ G_{ij}(t) - \frac{1}{z} \sum_{\boldsymbol{\rho}} G_{i+\boldsymbol{\rho},j}(t) \right\}, \quad (1.80)$$

where $M \equiv \langle S_i^z \rangle$. To solve this equation, we define

$$G_{\mathbf{k}}(\omega) \equiv \sum_{\mathbf{R}_{ij}} e^{-i\mathbf{k}\cdot\mathbf{R}_{ij}} \int_{-\infty}^{\infty} dt e^{i\omega t} G_{ij}(t), \quad (1.81)$$

where \mathbf{R}_i is the position vector of site i and $\mathbf{R}_{ij} \equiv \mathbf{R}_i - \mathbf{R}_j$. The inverse transformation is

$$G_{ij}(t) = \frac{1}{N} \sum_{\mathbf{k}} e^{i\mathbf{k}\cdot\mathbf{R}_{ij}} \int_{-\infty}^{\infty} \frac{d\omega}{2\pi} e^{-i\omega t} G_{\mathbf{k}}(\omega). \quad (1.82)$$

From Eqs. (1.80) and (1.82), we obtain

$$G_{\mathbf{k}}(\omega) = \frac{2M}{\omega - \epsilon_{\mathbf{k}}}, \quad (1.83)$$

where

$$\epsilon_{\mathbf{k}} \equiv zJM(1 - \gamma_{\mathbf{k}}), \quad (1.84)$$

$$\gamma_{\mathbf{k}} \equiv \frac{1}{z} \sum_{\boldsymbol{\rho}} e^{i\mathbf{k} \cdot \boldsymbol{\rho}}. \quad (1.85)$$

In the identical equation

$$\langle BA(t) \rangle = \frac{i}{2\pi} \int_{-\infty}^{\infty} d\omega e^{-i\omega t} \{G_{AB}^r(\omega) - G_{AB}^a(\omega)\} \frac{1}{e^{\beta\omega} - 1} \quad (1.86)$$

for the Green functions

$$G_{AB}^x(\omega) \equiv \int_{-\infty}^{\infty} dt e^{i\omega t} G_{AB}^x(t), \quad (1.87)$$

$$G_{AB}^R(t) \equiv -i\theta(t)\langle [A(t), B] \rangle, \quad (1.88)$$

$$G_{AB}^A(t) \equiv i\theta(-t)\langle [A(t), B] \rangle, \quad (1.89)$$

with $x = R$ and A , setting $A = S_i^+$ and $B = S_j^-$, we find

$$\langle S_j^- S_i^+(t) \rangle = \frac{i}{2\pi} \int_{-\infty}^{\infty} d\omega e^{-i\omega t} \{G_{ij}(\omega + i\eta) - G_{ij}(\omega - i\eta)\} \frac{1}{e^{\beta\omega} - 1}, \quad (1.90)$$

where η is the infinitesimal, i.e., $\eta = +0$. From Eq. (1.82), we obtain

$$\langle S_i^- S_i^+ \rangle = \frac{2M}{N} \sum_{\mathbf{k}} \frac{1}{e^{\beta\epsilon_{\mathbf{k}}} - 1}. \quad (1.91)$$

In the case of $S = 1/2$, because $\langle \mathbf{S}_i^2 \rangle = S(S+1) = 3/4$, $\langle (S_i^z)^2 \rangle = (\pm 1/2)^2 = 1/4$ and $\mathbf{S}_i^2 - (S_i^z)^2 = S_i^z + S_i^- S_i^+$, we obtain $\langle S^- S^+ \rangle = 1/2 - \langle S_i^z \rangle$.

Thus, Eq. (1.91) leads to the self-consistent equation for $S=1/2$:

$$\frac{1}{2M} = \frac{1}{N} \sum_{\mathbf{k}} \coth \left(\frac{\beta \epsilon_{\mathbf{k}}}{2} \right). \quad (1.92)$$

At sufficiently low temperatures, we obtain

$$M \simeq \frac{1}{2} - cT^{\frac{3}{2}}, \quad (1.93)$$

using the expansion $\gamma_{\mathbf{k}} \simeq 1 - Dk^2$ with a constant D for small $k \equiv |\mathbf{k}|$, where c is a constant.

The critical temperature T_c at which M vanishes is derived as

$$T_c = \frac{zJ}{4} \left(\frac{1}{N} \sum_{\mathbf{k}} \frac{1}{1 - \gamma_{\mathbf{k}}} \right)^{-1}. \quad (1.94)$$

In d -dimensional systems, the summation over \mathbf{k} can be replaced with the integral as

$$\frac{1}{N} \sum_{\mathbf{k}} \frac{1}{1 - \gamma_{\mathbf{k}}} = \frac{1}{N} \left(\frac{L}{2\pi} \right)^d \int d^d k \frac{1}{1 - \gamma_{\mathbf{k}}}, \quad (1.95)$$

where L is the linear dimension of the system, and the integral is taken over the 1st Brillouin zone. The integral diverges when $d = 1$ and 2 , but does not when $d = 3$:

$$\int d^1 k \frac{1}{1 - \gamma_{\mathbf{k}}} > 2 \int_0^{k_{\max}} dk k^{-2} = \infty, \quad (1.96)$$

$$\int d^2 k \frac{1}{1 - \gamma_{\mathbf{k}}} > \int_0^{2\pi} d\theta \int_0^{k_{\max}} dk k^{-1} = \infty, \quad (1.97)$$

$$\int d^3 k \frac{1}{1 - \gamma_{\mathbf{k}}} > \int_0^{2\pi} d\varphi \int_0^{\pi} d\theta \sin \theta \int_0^{k_{\max}} dk = 4\pi k_{\max}, \quad (1.98)$$

where k_{\max} is the upper limit of the region in which the approximation $\gamma_{\mathbf{k}} \simeq 1 - Dk^2$ is valid. Hence, the critical temperature is zero for one- and two-dimensional systems, which is consistent with the Mermin–Wagner theorem.

The function $\gamma_{\mathbf{k}}$ for the simple cubic (sc), body-centered cubic (bcc) and face-centered cubic (fcc) structure are expressed as

$$\gamma_{\mathbf{k}}^{\text{sc}} = \frac{1}{3} (\cos k^x + \cos k^y + \cos k^z), \quad (1.99)$$

$$\gamma_{\mathbf{k}}^{\text{bcc}} = \cos \frac{k^x}{2} \cos \frac{k^y}{2} \cos \frac{k^z}{2}, \quad (1.100)$$

$$\gamma_{\mathbf{k}}^{\text{fcc}} = \frac{1}{3} \left(\cos \frac{k^x}{2} \cos \frac{k^y}{2} + \cos \frac{k^y}{2} \cos \frac{k^z}{2} + \cos \frac{k^z}{2} \cos \frac{k^x}{2} \right), \quad (1.101)$$

respectively, where the lattice constant is taken to be unity. When k^μ is sufficiently small, we obtain approximate expressions

$$\gamma_{\mathbf{k}}^{\text{sc}} = 1 - \frac{1}{6}k^2, \quad (1.102)$$

$$\gamma_{\mathbf{k}}^{\text{bcc}} = 1 - \frac{1}{8}k^2, \quad (1.103)$$

$$\gamma_{\mathbf{k}}^{\text{fcc}} = 1 - \frac{1}{12}k^2. \quad (1.104)$$

The antiferromagnetic case

We examine the antiferromagnetic Heisenberg model

$$H = J \sum_{(i,j)} \mathbf{S}_i \cdot \mathbf{S}_j, \quad (1.105)$$

where $J > 0$ and $\mathbf{S}_i = (S_i^x, S_i^y, S_i^z)$ denotes the spin at site i .

In analogy with the ferromagnetic case, we find the expression for the Green function. To examine the antiferromagnetic order, we divide the lattice

into two sublattices A and B . We consider the retarded Green function

$$G_{ij}^X(t) \equiv \langle S_{i \in X}^+ | S_{j \in A}^- \rangle, \quad (1.106)$$

where $X = A, B$. From Eq. (1.76), the equations of motion for these Green functions are

$$i \frac{\partial}{\partial t} G_{ij}^X(t) = 2 \langle S_i^z \rangle \delta_{ij} \delta_{XA} \delta(t) - J \sum_{\rho} \langle (S_{i+\rho}^z S_i^+ - S_i^z S_{i+\rho}^+) | S_j^- \rangle \quad (1.107)$$

for $i \in X, j \in A$. Adopting the Tyablikov approximation given in Eqs. (1.78) and (1.79), we obtain

$$i \frac{\partial}{\partial t} G_{ij}^X(t) = 2M \delta_{ij} \delta_{XA} \delta(t) + (-1)^X z J M \left\{ G_{ij}^X(t) + \frac{1}{z} \sum_{\rho} G_{i+\rho, j}^{\bar{X}}(t) \right\}, \quad (1.108)$$

where $M \equiv \langle S_{l \in A}^z \rangle = -\langle S_{m \in B}^z \rangle$, which is assumed for the antiferromagnetic order. $(-1)^X$ is defined as $(-1)^A \equiv +1$, $(-1)^B \equiv -1$. To solve this equation, we define

$$G_{\mathbf{k}}^X(\omega) \equiv \sum_{\mathbf{R}_{ij}} e^{-i\mathbf{k} \cdot \mathbf{R}_{ij}} \int_{-\infty}^{\infty} dt e^{i\omega t} G_{ij}^X(t), \quad (1.109)$$

for sublattice X . The inverse transformation is

$$G_{ij}^X(t) = \frac{2}{N} \sum'_{\mathbf{k}} e^{i\mathbf{k} \cdot \mathbf{R}_{ij}} \int_{-\infty}^{\infty} \frac{d\omega}{2\pi} e^{-i\omega t} G_{\mathbf{k}}^X(\omega). \quad (1.110)$$

From Eqs. (1.109) and (1.110), we obtain

$$G_{\mathbf{k}}^A(\omega) = M \left(\frac{1 + g_{\mathbf{k}}}{\omega - \Delta_{\mathbf{k}}} + \frac{1 - g_{\mathbf{k}}}{\omega + \Delta_{\mathbf{k}}} \right), \quad (1.111)$$

$$G_{\mathbf{k}}^B(\omega) = -M \frac{\gamma_{\mathbf{k}}}{\sqrt{1 - \gamma_{\mathbf{k}}^2}} \left(\frac{1}{\omega - \Delta_{\mathbf{k}}} - \frac{1}{\omega + \Delta_{\mathbf{k}}} \right), \quad (1.112)$$

where

$$\Delta_{\mathbf{k}} \equiv zJM \sqrt{1 - \gamma_{\mathbf{k}}^2}, \quad (1.113)$$

$$g_{\mathbf{k}} \equiv \frac{1}{\sqrt{1 - \gamma_{\mathbf{k}}^2}}, \quad (1.114)$$

$$\gamma_{\mathbf{k}} \equiv \frac{1}{z} \sum_{\rho} e^{i\mathbf{k} \cdot \rho}. \quad (1.115)$$

From the identical equation given in Eq. (1.86), we find

$$\begin{aligned} & \langle S_{j \in A}^- S_{i \in X}^+(t) \rangle \\ &= \frac{i}{2\pi} \int_{-\infty}^{\infty} d\omega e^{-i\omega t} \{ G_{ij}^X(\omega + i\eta) - G_{ij}^X(\omega - i\eta) \} \frac{1}{e^{\beta\omega} - 1}, \end{aligned} \quad (1.116)$$

where η is the infinitesimal, i.e., $\eta = +0$. Taking the limit $t \rightarrow -0$ in Eq. (1.116), we obtain

$$\langle S_{l \in A}^- S_{i \in A}^+ \rangle = \frac{2M}{N} \sum_{\mathbf{k}} \left\{ -1 + \frac{1}{\sqrt{1 - \gamma_{\mathbf{k}}^2}} \coth \left(\frac{\beta \Delta_{\mathbf{k}}}{2} \right) \right\} \quad (1.117)$$

for $X = A$, $i = l \in A$, and $j = l' \in A$, and

$$\langle S_{l \in A}^- S_{m \in B}^+ \rangle = -\frac{2M}{N} \sum_{\mathbf{k}} \frac{\gamma_{\mathbf{k}}}{\sqrt{1 - \gamma_{\mathbf{k}}^2}} \coth \left(\frac{\beta \Delta_{\mathbf{k}}}{2} \right) e^{i\mathbf{k} \cdot \mathbf{R}_{ml}} \quad (1.118)$$

for $X = B$, $i = m \in B$, and $j = l \in A$.

In the case of $S = 1/2$, since $\langle \mathbf{S}_i^2 \rangle = S(S + 1) = 3/4$ and $\langle (S_i^z)^2 \rangle =$

$(\pm 1/2)^2 = 1/4$, we obtain $\langle S^- S^+ \rangle = 1/2 - \langle S_i^z \rangle$. Equation (1.117) leads to the self-consistent equation for $S = 1/2$:

$$\frac{1}{2M} = \frac{2}{N} \sum_{\mathbf{k}} \frac{1}{\sqrt{1 - \gamma_{\mathbf{k}}^2}} \coth \left(\frac{\beta \Delta_{\mathbf{k}}}{2} \right). \quad (1.119)$$

At sufficiently low temperatures, we obtain

$$M \simeq \frac{1}{2} - \Delta S - cT^2, \quad (1.120)$$

where c is a constant and ΔS is the shrinkage of spin expectation value at $T = 0$ due to the quantum effect, which is written as

$$\Delta S = \frac{1}{2} \left(1 - \frac{1}{W} \right) \quad (1.121)$$

with

$$W \equiv \frac{2}{N} \sum_{\mathbf{k}} \frac{1}{\sqrt{1 - \gamma_{\mathbf{k}}^2}}. \quad (1.122)$$

The critical temperature T_c at which M vanishes is derived as

$$T_c = \frac{zJ}{4} \left\{ \frac{1}{N} \sum_{\mathbf{k}} \left(\frac{1}{1 - \gamma_{\mathbf{k}}} + \frac{1}{1 + \gamma_{\mathbf{k}}} \right) \right\}^{-1}. \quad (1.123)$$

From Eqs. (1.95)–(1.98), the critical temperature is zero for one- and two-dimensional systems, which is consistent with the Mermin–Wagner theorem.

Chapter 2

Theoretical Model for the Insulating Phase in

λ -(BETS)₂FeCl₄

In this chapter, we define the coupled Heisenberg model and present the formulation of physical quantities on the basis of the Tyablikov approximation and the mean-field approximation. In this model, the system consists of two kinds of spins with different lengths. We call the spins with small and large lengths the small and large spins, respectively. The spins of each kind form two-dimensional layer, and these layers of the small and large spins are stacked alternately. The Hamiltonian includes three kinds of the exchange interactions: those between the small spins, those between the large spins, and those between the small and large spins. We derive the self-consistent equations for the sublattice magnetizations and the expression for the critical temperature.

The coupled Heisenberg model is

$$H = H_1 + H_2 + H_{12} \quad (2.1)$$

with

$$H_1 = \sum_{(i,j)} \sum_{\mu=x,y,z} J_1^\mu s_i^\mu s_j^\mu - \mathbf{h} \cdot \sum_i \mathbf{s}_i, \quad (2.2)$$

$$H_2 = \sum_{(i',j')} \sum_{\mu=x,y,z} J_2^\mu S_{i'}^\mu S_{j'}^\mu - \mathbf{h} \cdot \sum_{i'} \mathbf{S}_{i'}, \quad (2.3)$$

$$H_{12} = \sum_{(i,i')} \sum_{\mu=x,y,z} J_{12}^\mu s_i^\mu S_{i'}^\mu, \quad (2.4)$$

where $\mathbf{s}_i = (s_i^x, s_i^y, s_i^z)$ with length s at site i of lattice L_1 and $\mathbf{S}_{i'} = (S_{i'}^x, S_{i'}^y, S_{i'}^z)$ with length S at site i' of lattice L_2 . We assume that $s < S$. J_1^μ , J_2^μ and J_{12}^μ are positive coupling constants. $\mathbf{h} = (h_x, h_y, h_z)$ is a magnetic field. The sums $\sum_{(i,j)}$, $\sum_{(i',j')}$, and $\sum_{(i,i')}$ are taken over all pairs of the nearest neighbor sites in L_1 , those in L_2 , and those between L_1 and L_2 , respectively. In the antiferromagnetic phase, we divide the lattice L_ℓ into sublattices A_ℓ and B_ℓ . An example structure of the model is shown in Fig. 2.1.

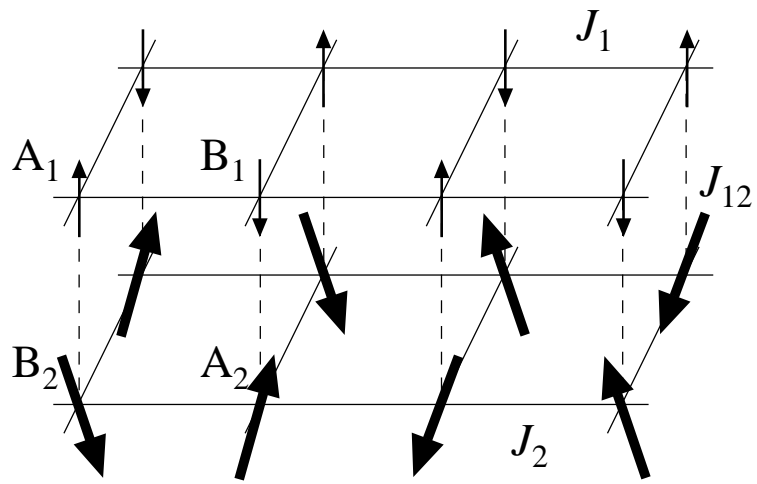


Figure 2.1: Example structure of the coupled Heisenberg model. The small and large arrows indicate the small and large spins, respectively. The solid lines indicate the lattices L_1 and L_2 . This figure is presented in Ref. [41].

Chapter 3

Analysis of the Low-Temperature Behavior

3.1 Low temperature limit

The Schottky model is given by

$$H = -\alpha \sum_i (-1)^i S_i^z - \mathbf{h} \cdot \sum_i \mathbf{S}_i, \quad (3.1)$$

where $\mathbf{S}_i = (S_i^x, S_i^y, S_i^z)$, $\mathbf{h} = (h_x, h_y, h_z)$, and α is a constant. We divide the lattice into sublattices A and B . We define notations

$$(-1)^i \equiv \begin{cases} +1 & \text{for } i \in A \\ -1 & \text{for } i \in B \end{cases} \quad (3.2)$$

$$(-1)^X \equiv \begin{cases} +1 & \text{for } X = A \\ -1 & \text{for } X = B \end{cases} . \quad (3.3)$$

For convenience, the sublattice magnetizations per site for sublattice X are defined as $M_X^\mu \equiv \langle S_i^\mu \rangle$, where $i \in X$. Expanding $M_X^\mu \equiv \langle S_i^\mu \rangle$ with respect to

h_μ , we find $M_X^\mu = M_X^{\mu(0)} + \Delta M_X^\mu + \dots$, where $M_X^{\mu(0)}$ and ΔM_X^μ are the 0th and 1st order terms, respectively. Thus, the spin susceptibilities per site for sublattice X and the total spin susceptibility per site are defined as

$$\chi_X^\mu \equiv \lim_{h_\mu \rightarrow 0} \frac{\Delta M_X^\mu}{h_\mu}, \quad (3.4)$$

$$\chi^\mu \equiv \frac{1}{2} (\chi_A^\mu + \chi_B^\mu). \quad (3.5)$$

In the case of $\mathbf{h} = (0, 0, h_z)$, the Hamiltonian given in Eq. (3.1) becomes

$$H = - \sum_i \{(-1)^i \alpha + h_z\} S_i^z. \quad (3.6)$$

Thus, we find

$$\begin{aligned} M_X^z &= S B_S(\beta \{(-1)^i \alpha + h_z\} S) \\ &= (-1)^i S B_S(\beta \alpha S) + \beta S^2 B'_S(\beta \alpha S) h_z + \dots, \end{aligned} \quad (3.7)$$

where $B_S(x)$ is the Brillouin function

$$B_S(x) \equiv \frac{2S+1}{2S} \coth\left(\frac{2S+1}{2S} x\right) - \frac{1}{2S} \coth\left(\frac{1}{2S} x\right) \quad (3.8)$$

and $B'_S(x) \equiv \partial B_S(x)/\partial x$. Therefore, we obtain

$$M_A^{z(0)} = -M_B^{z(0)} = S B_S(\beta \alpha S) \equiv M_0, \quad (3.9)$$

$$\chi^z = \chi_A^z = \chi_B^z = \beta S^2 B'_S(\beta \alpha S) \equiv \chi^\parallel. \quad (3.10)$$

In the case of $\mathbf{h} = (h_x, 0, 0)$, the Hamiltonian given in Eq. (3.1) becomes

$$\begin{aligned}
H &= - \sum_i \{(-1)^i \alpha S_i^z + h_x S_i^x\} \\
&= - \sum_{X=A,B} \sum_{i \in X} \{(-1)^X \alpha S_i^z + h_x S_i^x\} \\
&= - \sum_{X=A,B} \sum_{i \in X} (-1)^X \tilde{\alpha}_X S_i^{z'}, \tag{3.11}
\end{aligned}$$

where $S_i^{x'}$ and $S_i^{z'}$ are defined as

$$\begin{pmatrix} S_i^{z'} \\ S_i^{x'} \end{pmatrix} \equiv \begin{pmatrix} \cos \varphi_X & \sin \varphi_X \\ -\sin \varphi_X & \cos \varphi_X \end{pmatrix} \begin{pmatrix} S_i^z \\ S_i^x \end{pmatrix} \tag{3.12}$$

with

$$\cos \varphi_X \equiv \frac{\alpha}{\tilde{\alpha}_X}, \tag{3.13}$$

$$\sin \varphi_X \equiv (-1)^X \frac{h_x}{\tilde{\alpha}_X} \tag{3.14}$$

for $i \in X$. From Eqs. (3.11) and (3.12), we obtain

$$\begin{pmatrix} M_X^z \\ M_X^x \end{pmatrix} = \frac{1}{\tilde{\alpha}_X} S B_S(\beta \tilde{\alpha}_X S) \begin{pmatrix} (-1)^X \alpha \\ h_x \end{pmatrix}. \tag{3.15}$$

Expanding $\tilde{\alpha}_X$ with respect to h_x , we find $\tilde{\alpha}_X = \alpha + \Delta \tilde{\alpha}_X + \dots$, where α and $\Delta \tilde{\alpha}_X$ are the 0th and 1st order terms. Thus, we find

$$\begin{aligned}
&\frac{1}{\tilde{\alpha}_X} S B_S(\beta \tilde{\alpha}_X S) \\
&= \frac{1}{\alpha} \left[M_0 + \left\{ \beta S^2 B'_S(\beta \alpha S) - \frac{M_0}{\alpha} \right\} \Delta \tilde{\alpha}_X + \dots \right] \tag{3.16}
\end{aligned}$$

and

$$\Delta M_X^x = \frac{M_0}{\alpha} h_x. \quad (3.17)$$

Therefore, we obtain

$$\chi^x = \chi_A^x = \chi_B^x = \frac{M_0}{\alpha}. \quad (3.18)$$

We also obtain $\chi^y = \chi^x \equiv \chi^\perp$ from the symmetry of the system. The spin susceptibility in the direction of \mathbf{h} is given by

$$\chi(\theta) = \chi^\parallel \cos^2 \theta + \chi^\perp \sin^2 \theta, \quad (3.19)$$

where θ is the angle between z -axis and \mathbf{h} .

At $\mathbf{h} = 0$, the internal energy U is

$$U \equiv \langle H \rangle = -N\alpha M_0. \quad (3.20)$$

The specific heat C is

$$C \equiv \frac{\partial U}{\partial T} = Nk_B(\beta\alpha S)^2 B'_S(\beta\alpha S), \quad (3.21)$$

which is the $(2S + 1)$ -level Schottky-type specific heat.

3.2 Mean-field theory

In this section, we apply the mean-field approximation to the coupled Heisenberg model given in Eq. (2.1) and derive the expressions for sublattice magnetization, internal energy, specific heat, entropy and spin susceptibility.

We assume the easy axis is z -axis so that at zero magnetic field the sublattice magnetization in sublattice A is parallel to z -axis and that in B is antiparallel. The magnetic field is assumed to be oriented in xz plane, i.e., $\mathbf{h} = (h_x, 0, h_z)$. Applying the mean-field approximation, we obtain the mean-field Hamiltonian as

$$H_{\text{MF}} = \sum_{\ell=1,2} \sum_{X=A,B} \sum_{k \in X_\ell} \sum_{\mu=x,z} h_{\ell\mu}^X S_k^{\ell\mu} + (\text{const.}) \quad (3.22)$$

with the effective field

$$h_{\ell\mu}^X = \mathcal{J}_\ell^\mu M_{\ell\mu}^{\bar{X}} + \mathcal{J}_{12}^\mu M_{\ell\mu}^{\bar{X}} - h_\mu, \quad (3.23)$$

where $S_k^{\ell\mu}$ is μ component ($\mu = x, z$) of spin at site k in sublattice X_ℓ , i.e., $S_k^{1\mu} = s_k^\mu$ and $S_k^{2\mu} = S_k^\mu$, and $M_{\ell\mu}^X$ is μ component of the sublattice magnetization in sublattice X_ℓ , i.e., $M_{\ell\mu}^X = \langle S_k^{\ell\mu} \rangle$ for $k \in X_\ell$. $\mathcal{J}_\ell^\mu \equiv z_\ell J_\ell^\mu$ and $\mathcal{J}_{12}^\mu \equiv z_{12} J_{12}^\mu$ are defined, where z_ℓ and z_{12} are the number of nearest neighbour sites in subsystem ℓ and between subsystems 1 and 2, respectively. In the effective field shown in Eq. (3.23), the 1st and 2nd terms originate from the intrasubsystem and intersubsystem interactions, respectively.

To obtain the self-consistent equations, we rotate the coordinates as

$$\begin{pmatrix} S_k^{\ell z'} \\ S_k^{\ell x'} \end{pmatrix} = \begin{pmatrix} \cos \varphi_\ell^X & \sin \varphi_\ell^X \\ -\sin \varphi_\ell^X & \cos \varphi_\ell^X \end{pmatrix} \begin{pmatrix} S_k^{\ell z} \\ S_k^{\ell x} \end{pmatrix} \quad (3.24)$$

for $k \in X$. We choose φ_ℓ^X so that $M_{\ell x'}^X = 0$. Then, the mean-field Hamiltonian given in Eq. (3.22) is transformed into

$$H_{\text{MF}} = \sum_{\ell=1,2} \sum_{X=A,B} \sum_{k \in X_\ell} h_\ell^X S_k^{\ell z'} + (\text{const.}) \quad (3.25)$$

with $h_\ell^X = \sqrt{(h_{\ell x}^X)^2 + (h_{\ell z}^X)^2}$. From this Hamiltonian, we derive the self-consistent equations

$$M_{\ell z'}^X = -S_\ell B_{S_\ell}(\beta h_\ell^X S_\ell). \quad (3.26)$$

Using the rotation shown in Eq. (3.24) again, we obtain the self-consistent equations in the original coordinate as

$$M_{\ell\mu}^X = -\frac{h_{\ell\mu}^X}{h_\ell^X} S_\ell B_{S_\ell}(\beta h_\ell^X S_\ell). \quad (3.27)$$

Next, we examine the case of $\mathbf{h} = \mathbf{0}$. For the preparation, we expand $M_{\ell\mu}^X$, $h_{\ell\mu}^X$ and h_ℓ^X in powers of h_μ as

$$M_{\ell\mu}^X = M_{\ell\mu}^{X(0)} + \Delta M_{\ell\mu}^X + \dots, \quad (3.28)$$

$$h_{\ell\mu}^X = h_{\ell\mu}^{X(0)} + \Delta h_{\ell\mu}^X + \dots, \quad (3.29)$$

$$h_\ell^X = h_\ell^{X(0)} + \Delta h_\ell^X + \dots, \quad (3.30)$$

where $\Delta M_{\ell\mu}^X$, $\Delta h_{\ell\mu}^X$ and Δh_ℓ^X are the 1st order terms. From Eq. (3.23), we find

$$h_{\ell\mu}^{X(0)} = \mathcal{J}_\ell^\mu M_{\ell\mu}^{\bar{X}(0)} + \mathcal{J}_{12}^\mu M_{\bar{\ell}\mu}^{\bar{X}(0)}, \quad (3.31)$$

$$\Delta h_{\ell\mu}^X = \mathcal{J}_\ell^\mu \Delta M_{\ell\mu}^{\bar{X}} + \mathcal{J}_{12}^\mu \Delta M_{\bar{\ell}\mu}^{\bar{X}} - h_\mu. \quad (3.32)$$

The spontaneous sublattice magnetization $M_{\ell\mu}^{X(0)}$ in the antiferromagnetic phase are derived from the 0th order terms in the self-consistent equations

(3.27)

$$M_{\ell\mu}^{X(0)} = -\frac{h_{\ell\mu}^{X(0)}}{h_{\ell}^{X(0)}} S_{\ell} B_{S_{\ell}}(\beta h_{\ell}^{X(0)} S_{\ell}). \quad (3.33)$$

From the symmetry of the system, we find

$$M_{\ell z}^{A(0)} = -M_{\ell z}^{B(0)} \equiv M_{\ell 0} > 0, \quad (3.34)$$

$$h_{\ell z}^{B(0)} = -h_{\ell z}^{A(0)} = \mathcal{J}_{\ell} M_{\ell 0} + \mathcal{J}_{12} M_{\bar{\ell} 0} \equiv h_{\ell 0} > 0 \quad (3.35)$$

and $M_{\ell x}^{X(0)} = 0$, $h_{\ell x}^{X(0)} = 0$, $h_{\ell}^{X(0)} = \sqrt{(h_{\ell x}^{X(0)})^2 + (h_{\ell z}^{X(0)})^2} = h_{\ell 0}$. Therefore, we obtain the self-consistent equations of the sublattice magnetization $M_{\ell 0}$ as

$$M_{\ell 0} = S_{\ell} B_{S_{\ell}}(\beta h_{\ell 0} S_{\ell}). \quad (3.36)$$

In the paramagnetic phase, we obtain $M_{\ell\mu}^{X(0)} = 0$ as expected.

The critical temperature T_c at which $M_{\ell 0}$ vanishes in Eq. (3.36) is obtained as

$$T_c = \frac{1}{2} \left((T_{c1} + T_{c2}) + \sqrt{(T_{c1} - T_{c2})^2 + 4T_{c1}T_{c2} \frac{\mathcal{J}_{12}^2}{\mathcal{J}_1 \mathcal{J}_2}} \right) \quad (3.37)$$

with the critical temperatures of the independent subsystems $T_{c\ell} = \mathcal{J}_{\ell} S_{\ell} (S_{\ell} + 1)/3$. When \mathcal{J}_{12} is zero, the critical temperature is reduced to higher one of critical temperatures of the subsystems, i.e., $T_c = T_{c\ell}$ when $T_{c\ell} > T_{c\bar{\ell}}$.

The internal energy $U = \langle H \rangle$ is obtained as

$$\frac{U}{N} = -\frac{1}{2} \mathcal{J}_1 (M_{10})^2 - \frac{1}{2} \mathcal{J}_2 (M_{20})^2 - \mathcal{J}_{12} M_{10} M_{20} \quad (3.38)$$

because $\langle S_k^{\ell\mu} S_l^{\ell\mu} \rangle \simeq \langle S_k^{\ell\mu} \rangle \langle S_l^{\ell\mu} \rangle$ in the mean-field theory. The specific heat $C \equiv \partial E / \partial T$ is obtained as

$$\begin{aligned} \frac{C}{N} = & -\mathcal{J}_1 M_{10} \frac{\partial M_{10}}{\partial T} - \mathcal{J}_2 M_{20} \frac{\partial M_{20}}{\partial T} \\ & - \mathcal{J}_{12} \left(M_{10} \frac{\partial M_{20}}{\partial T} + \frac{\partial M_{10}}{\partial T} M_{20} \right). \end{aligned} \quad (3.39)$$

The entropy is given by

$$S = \int_0^T \frac{C}{T} dT. \quad (3.40)$$

The spin susceptibilities in the antiferromagnetic phase are derived from the 1st order terms in the self-consistent equations given in Eq. (3.27)

$$\begin{aligned} h_{\ell 0} \Delta M_{\ell\mu}^X + M_{\ell 0} \Delta h_{\ell\mu}^X \\ + \left\{ M_{\ell\mu}^{X(0)} + \beta h_{\ell\mu}^{X(0)} (S_\ell)^2 B'_{S_\ell}(\beta h_{\ell 0} S_\ell) \right\} \Delta h_\ell^X = 0. \end{aligned} \quad (3.41)$$

In the case of $\mathbf{h} = (0, 0, h_z)$, using $\Delta h_\ell^X = \text{sgn}(h_\ell^{X(0)}) \Delta h_{\ell z}^X$, Eq. (3.41) reduces to

$$\left\{ \beta (S_\ell)^2 B'_{S_\ell}(\beta h_{\ell 0} S_\ell) \right\}^{-1} \Delta M_{\ell z}^X + \mathcal{J}_\ell \Delta M_{\ell z}^{\bar{X}} + \mathcal{J}_{12} \Delta M_{\ell z}^{\bar{X}} = h_z. \quad (3.42)$$

In the case of $\mathbf{h} = (h_x, 0, 0)$, Eq. (3.41) reduces to

$$\frac{h_{\ell 0}}{M_{\ell 0}} \Delta M_{\ell x}^X + \mathcal{J}'_\ell \Delta M_{\ell x}^{\bar{X}} + \mathcal{J}'_{12} \Delta M_{\ell x}^{\bar{X}} = h_x. \quad (3.43)$$

On the other hand, the spin susceptibilities in the paramagnetic phase are

derived from the 1st order terms

$$\frac{T}{T_{cl}} \mathcal{J}_\ell \Delta M_{\ell\mu}^X + \mathcal{J}_\ell^\mu \Delta M_{\ell\mu}^{\bar{X}} + \mathcal{J}_{12}^\mu \Delta M_{\ell\mu}^{\bar{X}} = h_\mu \quad (3.44)$$

because $M_{\ell\mu}^{X(0)} = 0$, $h_{\ell\mu}^{X(0)} = 0$ and $h_\ell^{X(0)} = 0$. Solving Eqs.(3.42)–(3.44), we obtain the spin susceptibilities as

$$\chi_\ell^\mu \equiv \lim_{h_\mu \rightarrow 0} \frac{\Delta M^{\ell\mu}}{h_\mu} = \chi_{\ell 0}^\mu \frac{1 - \mathcal{J}_{12}^\mu \chi_{\ell 0}^\mu}{1 - (\mathcal{J}_{12}^\mu)^2 \chi_{10}^\mu \chi_{20}^\mu}, \quad (3.45)$$

using $\Delta M_{\ell\mu} = (\Delta M_{\ell\mu}^A + \Delta M_{\ell\mu}^B)/2$, where $\chi_{\ell 0}^\mu$ is defined as

$$\chi_{\ell 0}^z = \frac{1}{\beta(S_\ell)^2 B'_{S_\ell}(\beta h_{\ell 0} S_\ell) + \mathcal{J}_\ell}, \quad (3.46)$$

$$\chi_{\ell 0}^x = \frac{1}{\mathcal{J}_\ell + \mathcal{J}'_\ell + \mathcal{J}_{12}(M_{\bar{\ell} 0}/M_{\ell 0})} \quad (3.47)$$

in the antiferromagnetic phase and

$$\chi_{\ell 0}^\mu = \frac{S_\ell(S_\ell + 1)/3}{T + (\mathcal{J}_\ell^\mu/\mathcal{J}_\ell)T_{cl}} \quad (3.48)$$

in the paramagnetic phase.

3.3 Results

3.3.1 Some typical cases

We study the thermodynamic and magnetic properties of the coupled Heisenberg model on the basis of the mean-field approximation. Figure 3.1 shows the temperature dependence of the sublattice magnetizations M_1 and M_2 and the specific heat C . For $\mathcal{J}_{12} = 0$, the sublattice magnetization and specific heat are the summations of those of two simple Heisenberg models with different

spin lengths. In this case, two phase transitions of subsystems occur successively. Two sublattice magnetizations vanish at different temperatures, and the specific heat has the two cusps. The specific heat of subsystem ℓ is given by

$$\frac{C_\ell}{Nk_B} = -\mathcal{J}_\ell M_{\ell 0} \frac{\partial M_{\ell 0}}{\partial T}. \quad (3.49)$$

For $\mathcal{J}_{12} \neq 0$, only one phase-transition occurs at T_c of Eq. (3.37): M_2 becomes finite even above T_{c2} because of non-zero M_1 , and in the specific heat the cusp at lower temperature broaden as \mathcal{J}_{12} increases, as shown in Fig. 3.1.

3.3.2 Reproduction of experimental results

We reanalyze the specific heat and spin susceptibility in λ -(BETS)₂FeCl₄ on the basis of the mean-field model. For the specific heat, we assume three models in low, intermediate, and high temperature regions and estimate the model parameters \mathcal{J}_1 , \mathcal{J}_2 , and \mathcal{J}_{12} using the least-squares method, where we calculate the root-mean-square-residual (RMSR) σ . For the spin susceptibility, we examine the four limiting cases with respect to the anisotropies of \mathcal{J}_2^μ and \mathcal{J}_{12}^μ . We estimate the angle θ between z -axis and c -axis, and examine the origin of the magnetic anisotropy.

The specific heat

We define the RMSR σ for the specific heat as

$$\sigma(T_{\text{ul}}) \equiv \left[\sum_{i=1}^{N_{\text{ul}}} \frac{\Delta T_i}{T_{\text{ul}}} \left(\frac{C^{\text{th}}(T_i)}{Nk_B} - \frac{C^{\text{exp}}(T_i)}{Nk_B} \right)^2 \right]^{1/2} \quad (3.50)$$

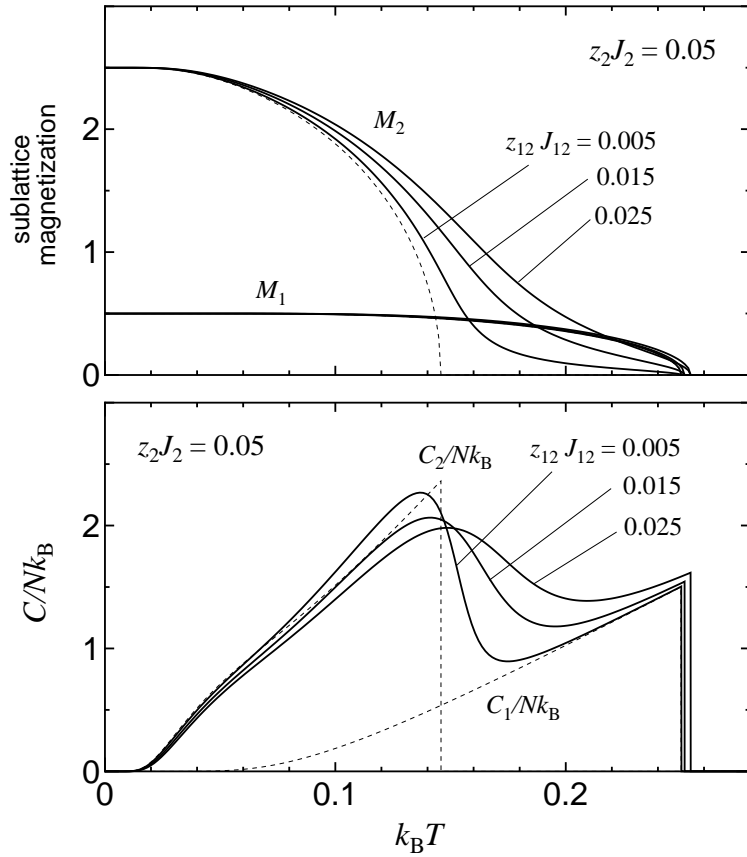


Figure 3.1: Temperature dependence of the sublattice magnetizations M_1 and M_2 and the specific heat C for $\mathcal{J}_1 = 1$. The dotted curves indicate the results of $\mathcal{J}_{12} = 0$. C_ℓ is the specific heat of the subsystem ℓ of Eq. (3.49). This figure is presented in Ref. [41].

for a temperature region $[0, T_{\text{ul}}]$, where ΔT_i is the temperature interval defined as

$$\Delta T_i \equiv \begin{cases} \frac{T_2}{2} & \text{for } i = 1 \\ \frac{T_{i+1} - T_{i-1}}{2} & \text{for } 1 < i < N_{\text{ul}} \\ \frac{T_{N_{\text{ul}}} - T_{N_{\text{ul}}-1}}{2} & \text{for } i = N_{\text{ul}} \end{cases}, \quad (3.51)$$

with $T_{\text{ul}} = T_{N_{\text{ul}}}$. Here, T_i is the temperature of the data point i , and N_{ul} is the number of the data points in a temperature region $[0, T_{\text{ul}}]$. $C^{\text{th}}(T_i)$ and $C^{\text{exp}}(T_i)$ are the theoretical and experimental values of the specific heat in units of Nk_{B} at the temperature T_i , respectively. From Eq. (3.51), it is verified that

$$T_{\text{ul}} = \sum_{i=1}^{N_{\text{ul}}} \Delta T_i. \quad (3.52)$$

In Eq. (3.51), ΔT_i is not constant because the distribution of the experimental data point is not uniform. If ΔT_i is constant as $\Delta T_i = T_{\text{ul}}/N_{\text{ul}}$, Eq. (3.50) reduces to the usual RMSR. We refer to the minimum σ given by optimum model parameter as σ_{min} .

We reanalyze the specific-heat data by Akiba et al. [17]. We start from the data near $T = 0$, where the shrinkage of the sublattice magnetizations are sufficiently small, i.e., $M_{\ell 0} \approx S_{\ell}$. Thus, we obtain the Schottky model

$$H \simeq H_{\text{MF}}^{\text{Sch}} \equiv - \sum_{X=A,B} \sum_{i \in X_2} (-1)^X \Delta_{\text{d}} S_i^z, \quad (3.53)$$

where $\Delta_{\text{d}} \equiv \mathcal{J}_2 S_2 + \mathcal{J}_{12} S_1$ is a constant exchange field. According to Eq. (3.21),

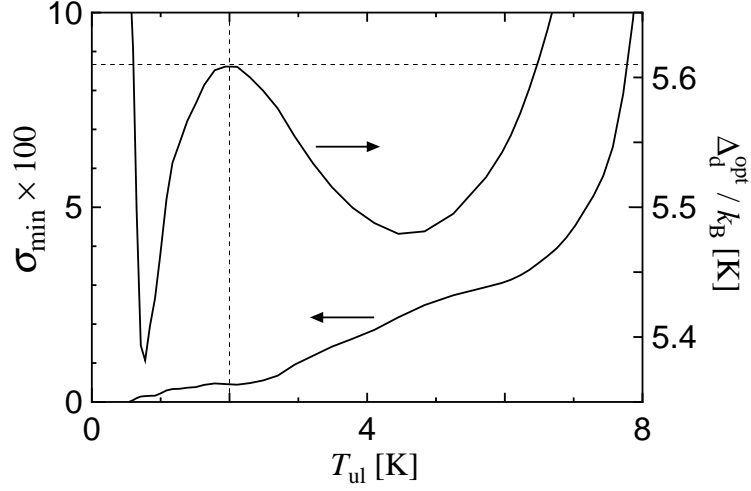


Figure 3.2: Minimum RMSR σ_{\min} and optimum parameter Δ_d^{opt} for $H_{\text{MF}}^{\text{Sch}}$. The horizontal and vertical dotted lines indicate 5.61 K and 2 K, respectively. This figure is presented in Ref. [41].

the specific heat C is

$$C \simeq Nk_B(\beta\Delta_d S)^2 B'_S(\beta\Delta_d S), \quad (3.54)$$

which is the six-level Schottky-type specific heat. Regarding Δ_d as a fitting parameter, we obtain σ_{\min} and the optimum Δ_d for each T_{ul} , which are shown in Fig. 3.2. Below 2.2 K, σ_{\min} is so small that $H_{\text{MF}}^{\text{Sch}}$ can be regarded as an effective model. However, below 1.8 K, Δ_d^{opt} varies significantly because the number of the data points is small. Near 2 K, Δ_d^{opt} is saturated, and thus we regard this saturated value of Δ_d^{opt} as the true value. Therefore, we obtain

$$\Delta_d \approx 5.61 \text{ K}. \quad (3.55)$$

In Fig. 3.2, above 2.5 K, σ_{\min} increases and Δ_d^{opt} decreases, which implies that the shrinkage of M_{20} is not small. Thus, above 2.5 K the Schottky model is invalid. Taking into account only the shrinkage of the large spins,

the effective Hamiltonian is

$$H \simeq H'_{\text{MF}} \equiv - \sum_{X=A,B} \sum_{i \in X_2} (-1)^X \alpha'_2 S_i^z \quad (3.56)$$

with $\alpha'_1 \equiv \mathcal{J}_1 S_1 + \mathcal{J}_{12} M_{20}$ and $\alpha'_2 \equiv \mathcal{J}_2 M_{20} + \mathcal{J}_{12} S_1$. Thus, $M_{10} \approx S_1$, and M_{20} is obtained by the self-consistent equation

$$M_{20} = S_2 B_{S_2}(\beta \alpha'_2 S_2). \quad (3.57)$$

Equation (3.57) coincides with Eq. (3.36) in the limit of $\mathcal{J}_1/k_B T \rightarrow \infty$. According to Eq. (3.39), the specific heat C is

$$\frac{C}{Nk_B} \simeq -\mathcal{J}_2 M_{20} \frac{\partial M_{20}}{\partial T} - \mathcal{J}_{12} S_1 \frac{\partial M_{20}}{\partial T}. \quad (3.58)$$

Regarding \mathcal{J}_2 and \mathcal{J}_{12} as fitting parameters, we obtain σ_{min} under the condition given in Eq. (3.55). As shown in Fig. 3.3, below 6 K, σ_{min} is so small that H'_{MF} can be regarded as an effective model. The σ_{min} of $H_{\text{MF}}^{\text{Sch}}$ is smaller than that of H'_{MF} , which implies that the approximation is improved significantly. Below 3 K, $\mathcal{J}_{12}^{\text{opt}}$ varies largely because the shrinkage of M_{20} is too small for $\mathcal{J}_{12}^{\text{opt}}$ to be determined. We find the saturated part of $\mathcal{J}_{12}^{\text{opt}}$ for $3.5 \text{ K} \lesssim T_{\text{ul}} \lesssim 6 \text{ K}$ and adopt it as the true value. Therefore, we obtain

$$\begin{aligned} \mathcal{J}_{12} &\approx 9.3 \text{ K}, \\ \mathcal{J}_2 &\approx 0.384 \text{ K}. \end{aligned} \quad (3.59)$$

In Fig. 3.3, above 6 K, since σ_{min} is not so small, H'_{MF} is not justified. Taking into account not only the shrinkage of M_{20} but also M_{10} , we calculate σ_{min} and the optimum \mathcal{J}_1 for the mean-field model H_{MF} under the condition

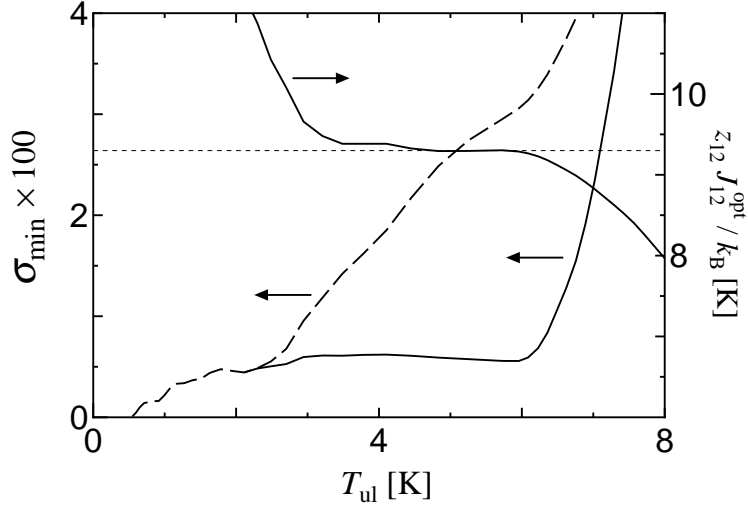


Figure 3.3: Minimum RMSR σ_{\min} and optimum parameter $\mathcal{J}_{12}^{\text{opt}}$ for H'_{MF} . The horizontal dotted lines indicate $\mathcal{J}_{12}^{\text{opt}} = 9.3$ K. This figure is presented in Ref. [41].

given in Eq. (3.59). M_{10} and M_{20} are obtained from the self-consistent equations given in Eq. (3.36). As shown in Fig. 3.4, below 6 K, σ_{\min} of H'_{MF} and that of H_{MF} almost coincide. σ_{\min} of H_{MF} is small below 6.8 K, increases significantly above 6.8 K, and becomes large above 7.4 K. $\mathcal{J}_1^{\text{opt}}$ is not saturated because H_{MF} ignores the fluctuation near $T_c = 8.3$ K. The rate of decrease of $\mathcal{J}_1^{\text{opt}}$ decreases below 6.5 K and increases above 7.4 K, which implies that the critical fluctuation increases before the saturation. Therefore, probably, the value of $\mathcal{J}_1^{\text{opt}}$ for $6.5 \text{ K} \lesssim T_{\text{ul}} \lesssim 7.4 \text{ K}$ is the true value, and thus we obtain

$$60 \text{ K} \lesssim \mathcal{J}_1 \lesssim 80 \text{ K}. \quad (3.60)$$

Above 7.4 K, both σ_{\min} and the rate of decrease of $\mathcal{J}_1^{\text{opt}}$ increase. Therefore, the mean-field theory completely breaks down. Figure 3.5 shows the \mathcal{J}_1 dependence of RMSR σ . Below 60 K, σ_{\min} increases rapidly as \mathcal{J}_1 decreases, which implies that $\mathcal{J}_1 \gtrsim 60$ K.

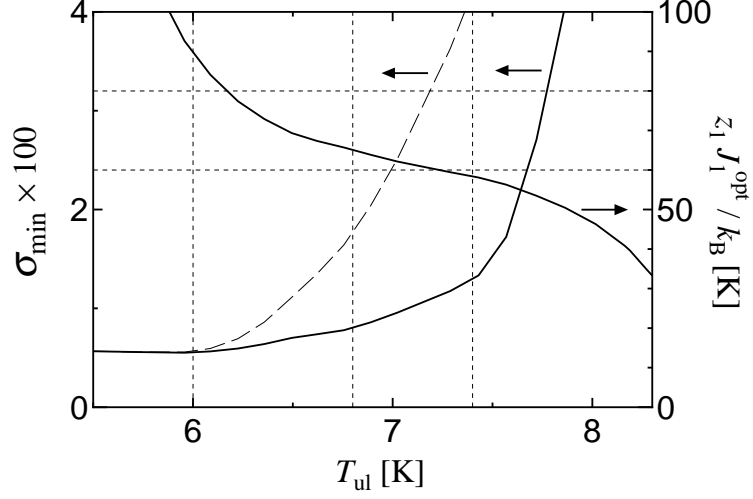


Figure 3.4: Minimum RMSR σ_{\min} and optimum parameter $\mathcal{J}_1^{\text{opt}}$ for H_{MF} . The horizontal and vertical dotted lines indicate 80, 60, 6, 6.8, and 7.4 K, respectively. This figure is presented in Ref. [41].

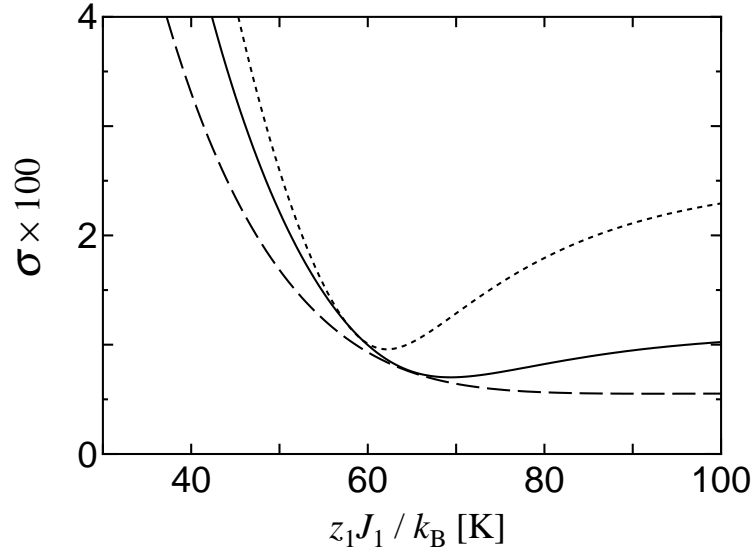


Figure 3.5: \mathcal{J}_1 dependence of RMSR σ for H_{MF} . $\mathcal{J}_2 = 0.384$ K and $\mathcal{J}_{12} = 9.3$ K are fixed. The solid, dashed, and dotted curves are the results for $T_{\text{ul}} = 6.5, 6,$ and 7 K, respectively. This figure is presented in Ref. [41].

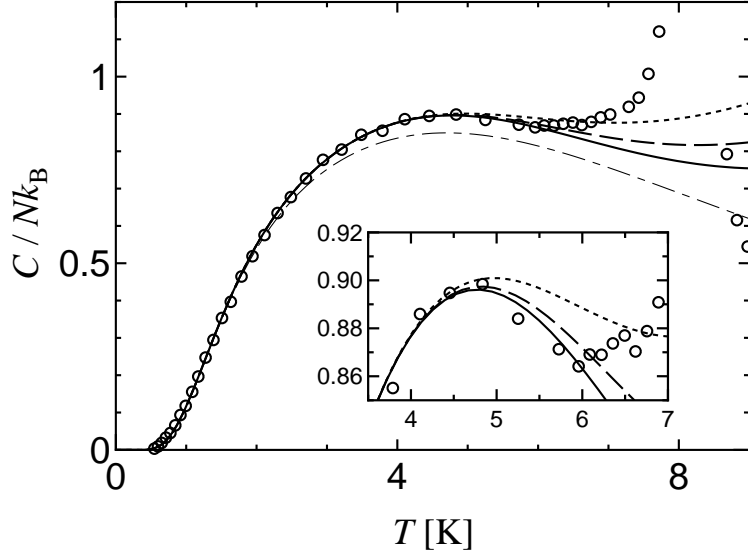


Figure 3.6: Temperature dependence of the specific heat. The circles are the experimental data in λ -(BETS) $_2$ FeCl $_4$ by Akiba et al. [17]. The solid, dashed, and dotted curves are the theoretical result of $\mathcal{J}_1 = 80, 70,$ and 60 K, respectively. $\mathcal{J}_2 = 0.384$ K and $\mathcal{J}_{12} = 9.3$ K are fixed. The thin dot-dashed curve is the result of the Schottky model with $\Delta_d = 5.61$ K. The thin dotted vertical line indicates $T_c \approx 8.3$ K. This figure is presented in Ref. [41].

Figure 3.6 shows the comparison between the theoretical curves and the experimental data. The curves of $\mathcal{J}_1 = 70$ and 80 K give good agreement below 6 K, that of $\mathcal{J}_1 = 60$ K gives the best below 7 K. Compared with the curve of Schottky model, the mean-field model improves the results significantly because the temperature dependences of the exchange fields are taken into account. The Schottky model does not reproduce the height of the peak because the parameter Δ_d affects the only horizontal scale but not the vertical scale.

In Eq. (3.60), we improve the lower limit of \mathcal{J}_1 from Fig. 3.6. The theoretical curve should be smaller than the experimental data because the specific heat is proportional to the fluctuation of the energy, and the mean-field model ignores the fluctuation. Therefore, if the experimental error ΔC is smaller

than $0.02Nk_B$, the curve of $\mathcal{J}_1 = 60K$ is inadequate. Thus, $\mathcal{J}_1 \gtrsim 70K$ is obtained. Similarly, if ΔC is smaller than $0.01Nk_B$, $\mathcal{J}_1 \gtrsim 80K$ is estimated.

The spin susceptibility

We investigate the spin susceptibility of λ -(BETS)₂FeCl₄ using the experimental data by Akiba et al. [18]. We find the values of the coupling constants \mathcal{J}_2^x and \mathcal{J}_{12}^x , and the angle θ between the easy axis and c -axis. We define the RMSR

$$\sigma_\chi(r_2, r_{12}) \equiv \left[\frac{1}{N_{\text{ul}}} \sum_{i=1}^{N_{\text{ul}}} (\chi_{\text{mag}}^{\text{th}}(r_2, r_{12}, \theta, T_i) - C_\chi \chi_{\text{mag}}^{\text{exp}}(T_i))^2 \right]^{1/2}, \quad (3.61)$$

where $r_2 \equiv \mathcal{J}_2^x/\mathcal{J}_2$, $r_{12} \equiv \mathcal{J}_{12}^x/\mathcal{J}_{12}$, and C_χ is a constant multiplier due to the experimental technique. Here, the weight $1/N_{\text{ul}}$ is constant unlike $\Delta T_i/T_{\text{ul}}$ in the RMSR for the specific heat given in Eq. (3.50) because the distribution of the data points is almost uniform, and the absence of the data points below 2 K gives the too large weight $\Delta T_i/T_{\text{ul}}$ of the leftmost point.

We examine the four cases of $(r_2, r_{12}) = (0, 0)$, $(1, 0)$, $(0, 1)$ and $(1, 1)$, where r_2 and r_{12} are equal to 0 and 1 correspond to anisotropic and isotropic limits, respectively. For $\theta \approx 30^\circ$ given by the magnetic torque experiments [11, 36], $(r_2, r_{12}) = (1, 0)$ minimizes σ_χ . For $(r_2, r_{12}) = (1, 0)$, the best parameters are $\theta \approx 26.6^\circ$ and $C_\chi \approx 1.22$, which gives $\sigma_\chi \approx 4.1 \times 10^{-4} \text{ K}^{-1}$. Similarly, $(r_2, r_{12}) = (0, 0)$, $(0, 1)$ and $(1, 1)$ give the best parameters $\theta = 24.6^\circ$, 22.9° , and 25.3° , respectively. Figure 3.7 shows the theoretical results and experimental data. The curve of $(r_2, r_{12}) = (1, 0)$ and $\theta = 26.6^\circ$ agrees with the experimental data. For $\theta = 27^\circ$, we obtain \mathcal{J}_{12}^μ is anisotropic, and \mathcal{J}_2^μ is isotropic. Therefore, the origin of the magnetic anisotropy is \mathcal{J}_{12}^μ rather than \mathcal{J}_2^μ .

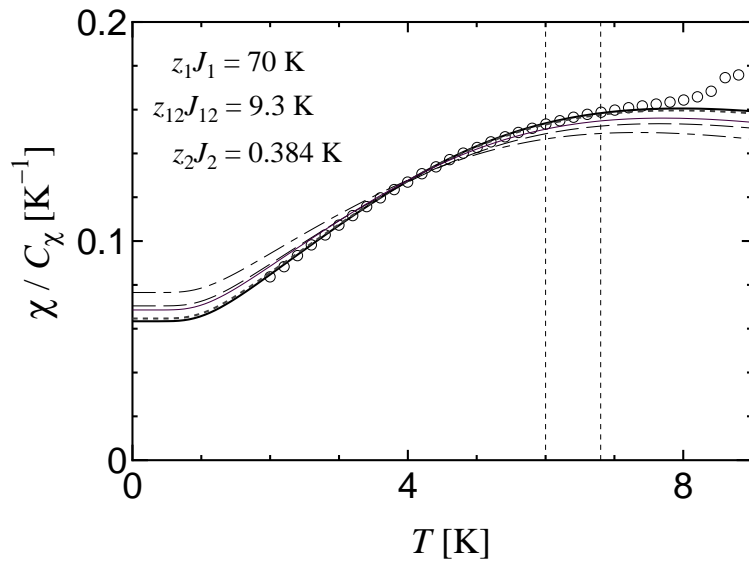


Figure 3.7: Temperature dependence of the spin susceptibility. The circles are the experimental data of λ -(BETS) $_2$ FeCl $_4$ by Akiba et al. [18], respectively. The solid and dotted curves are the theoretical results of $\theta = 26.6^\circ$ and 27° for $(r_2, r_{12}) = (1, 0)$, respectively. The thin solid, dashed, and dot-dashed curves are the results of $(r_2, r_{12}) = (1, 1)$, $(0, 0)$, and $(0, 1)$ for $\theta = 27^\circ$, respectively. This figure is presented in Ref. [41].

Table 3.1: The values of RMSR $\sigma_\chi(r_2, r_{12})$. $\mathcal{J}_1 = 70$ K, $\mathcal{J}_2 = 0.384$ K, and $\mathcal{J}_{12} = 9.30$ K are adopted from the result of the specific-heat. This table is presented in Ref. [41].

θ	32°	31°	30°	27°	26°
$\sigma_\chi(0, 0)$	12.5	10.7	8.9	3.8	2.2
$\sigma_\chi(1, 0)$	8.1	6.5	5.0	0.68	0.94
$\sigma_\chi(0, 1)$	17.1	15.0	13.0	7.2	5.3
$\sigma_\chi(1, 1)$	10.9	9.1	7.5	2.6	1.1

3.4 Summary of the chapter

In this chapter, we examined the antiferromagnetic coupled Heisenberg model on the basis of the mean-field approximation. We derived the self-consistent equations for the sublattice magnetizations and the expression of the spin susceptibility. We reanalyzed the temperature dependence of the specific heat and spin susceptibility in λ -(BETS)₂FeCl₄ using the least-squares method.

For $h = 0$, we examined three effective models for high, intermediate, and low temperature regions. As a result, we obtained the parameters $\Delta_d \approx 5.6$ K, $\mathcal{J}_{12} \approx 9.3$ K, $\mathcal{J}_2 \approx 0.4$ K, and $\mathcal{J}_1 \gtrsim 60$ K. If the error of the experiment is sufficiently small, we can narrow down the condition of \mathcal{J}_1 as $\mathcal{J}_1 \gtrsim 80$ K. The approximations $M_2 \approx S_2$ and $M_1 \approx S_1$ are appropriate below 2 K and 6 K, which correspond the energy scales $\Delta_d/3 \approx 2$ K and $T_{c1}/3 \approx 5$ K - 6 K, respectively. Therefore, only 3d spins fluctuate significantly for 2 K $\lesssim T \lesssim 6$ K.

We shall compare the present result with the estimations by other methods. The relation $J_1 \gg J_{12} \gg J_2$ is consistent with the result of Hückel method by Mori and Katsuhara [12]. However, with respect to the magnitudes of the coupling constants, the present estimates do not agree with those of the previous theories: $\mathcal{J}_1 = 448$ K, $\mathcal{J}_{12} = 14.62$ K, $\mathcal{J}_2 = 0.64$ K by Mori and Katsuhara, $J_{12} \sim 25$ K by Hotta and Fukuyama [38], and $J_2 = 55$ K,

$J_{12} = 88$ K by Brossard et al. [7]. These differences are probably because the present coupling constants are effective parameters in the simplified model that are different from more microscopic values. Furthermore, the estimation based on the microscopic theory is difficult. For example, up to the 2nd-order perturbation with respect to hopping integrals, the perturbation theory is not accurate.

λ -(BETS)₂FeCl₄ has also been studied as a magnetic-field-induced superconductor, which shows the maximum transition temperature $B_{\text{cent}} \approx 33$ T [9, 24]. According to the Jaccarino–Peter compensation effect [27], this magnetic flux density is compensated by the exchange field. This consideration and the value of B_{cent} are supported by the NMR measurement [42] and Shubnikov–de Hass oscillations [10, 39]. In this mechanism, we obtain that $\mathcal{J}_{12}S_2/2 = \mu_e B_{\text{cent}}$, where μ_e is the electron magnetic moment. Thus, we find that $\mathcal{J}_{12} \approx 17.8$ K and $\Delta_d > \mathcal{J}_{12}S_1 \approx 8.9$ K, where the g -factor is assumed to be 2. The value of Δ_d disagree with the present result of the Schottky model. Therefore, the effective coupling constant in the localized spin model can be used only in the antiferromagnetic insulator phase but not in the high-field metallic phase.

For $h \neq 0$, we reanalyzed the spin susceptibility of λ -(BETS)₂FeCl₄. It was found that the magnetic anisotropy originates from \mathcal{J}_{12}^μ rather than \mathcal{J}_2^μ for $\theta \approx 30^\circ$ based on the magnetic torque experiment [36]. The spin susceptibility is reproduced better for $\theta \approx 26 - 27^\circ$ than for $\theta \approx 30^\circ$.

In conclusion, the mean-field model reproduces the specific heat and spin susceptibility in λ -(BETS)₂FeCl₄ below 6 – 6.8 K. We obtain $\mathcal{J}_1 \gg \mathcal{J}_{12} \gg \mathcal{J}_2$. Hence, the present model gives a specific heat similar to Schottky-type specific heat. In the mean-field model, the resultant specific heat is not accurate above 6.8 K. In particular, the model becomes completely inappropriate

above 7.4 K because the mean-field approximation and/or localized spin picture breaks down. The detailed study of the phase transition beyond the localized spin picture is left for the future.

Chapter 4

Phase Transition

—Stabilization Mechanism of Antiferromagnetic Order—

4.1 Extension of the Tyablikov approximation

In this section, we apply the Tyablikov approximation to the coupled Heisenberg model given in Eq. (2.1), assuming that the exchange interactions between the small spins are isotropic, i.e., $J_1^x = J_1^y = J_1^z \equiv J_1$, and that the others are anisotropic. We derive the self-consistent equations for the sublattice magnetizations and the expression of the critical temperature.

Assuming that the fluctuation of the large spins is sufficiently small, we apply the mean-field approximation to the large spins. Thus, the Hamilto-

nian is approximately expressed as

$$H \simeq \tilde{H}_1 + \tilde{H}_2 \quad (4.1)$$

with

$$\tilde{H}_1 = H_1 - \sum_i (-1)^i \alpha_{10} \delta_1 s_i^z, \quad (4.2)$$

$$\tilde{H}_2 = - \sum_{i'} (-1)^{i'} \alpha_2 S_{i'}^z, \quad (4.3)$$

where the exchange fields α_1 and α_2 are

$$\alpha_1 = z_1 J_1 m + z_{12} J_{12} M, \quad (4.4)$$

$$\alpha_2 = z_2 J_2 M + z_{12} J_{12} m, \quad (4.5)$$

which are expressed as $\alpha_\ell = \alpha_{\ell 0}(1 + \delta_\ell)$ with $\alpha_{10} = z_1 J_1 m$, $\alpha_{20} = z_2 J_2 M$, $\delta_1 = z_{12} J_{12} M / z_1 J_1 m$, and $\delta_2 = z_{12} J_{12} m / z_2 J_2 M$. The sublattice magnetizations are defined by $m \equiv \langle s_{i \in A}^z \rangle = -\langle s_{m \in B}^z \rangle$ and $M \equiv \langle S_{i' \in A}^z \rangle = -\langle S_{m' \in B}^z \rangle$. We define the notations

$$(-1)^k \equiv \begin{cases} +1 & \text{for } k \in A_\ell \\ -1 & \text{for } k \in B_\ell \end{cases} \quad (4.6)$$

$$(-1)^X \equiv \begin{cases} +1 & \text{for } X = A \\ -1 & \text{for } X = B \end{cases} . \quad (4.7)$$

From Eqs. (4.1)–(4.3), we obtain the self-consistent equation

$$M = S B_S(\beta \alpha_2 S). \quad (4.8)$$

We define the Green function as

$$D_{ij}^{XA}(\tau) \equiv -\langle T_\tau[s_i^+(\tau)s_j^-] \rangle, \quad (4.9)$$

where $\hat{A}(\tau) \equiv e^{\tau H} \hat{A} e^{-\tau H}$, and $T_\tau[\hat{A}(\tau)\hat{B}] \equiv \hat{A}(\tau)\hat{B} \theta(\tau) + \hat{B}\hat{A}(\tau) \theta(-\tau)$. The Green function satisfies the equations of motion

$$-\frac{\partial}{\partial \tau} D_{ij}^{XA}(\tau) = (-1)^i 2m \delta_{ij} \delta(\tau) + \langle T_\tau[[H, s_i^+(\tau)]s_j^-] \rangle. \quad (4.10)$$

From Eqs. (4.1)–(4.3), we find

$$\begin{aligned} & \langle T_\tau[[H, s_i^+(\tau)]s_j^-] \rangle \\ &= J_1 \sum_{\boldsymbol{\rho}} \langle T_\tau[(s_{i+\boldsymbol{\rho}}^z s_i^+ - s_{i+\boldsymbol{\rho}}^+ s_i^z)_\tau s_j^-] \rangle + (-1)^i \alpha_{10} \delta_1 D_{ij}^{XA}(\tau). \end{aligned} \quad (4.11)$$

By adopting the Tyablikov approximation

$$\langle T_\tau[(s_{i+\boldsymbol{\rho}}^z s_i^+)_\tau s_j^-] \rangle \simeq \langle s_{i+\boldsymbol{\rho}}^z \rangle \langle T_\tau[s_i^+(\tau)s_j^-] \rangle, \quad (4.12)$$

$$\langle T_\tau[(s_{i+\boldsymbol{\rho}}^+ s_i^z)_\tau s_j^-] \rangle \simeq \langle s_i^z \rangle \langle T_\tau[s_{i+\boldsymbol{\rho}}^+(\tau)s_j^-] \rangle, \quad (4.13)$$

we rewrite Eq. (4.10) as

$$\begin{aligned} & -(-1)^i \frac{\partial}{\partial \tau} D_{ij}^{XA}(\tau) \\ &= 2m \delta_{ij} \delta(\tau) + \alpha_1 D_{ij}^{XA}(\tau) + \alpha_{10} \frac{1}{z_1} \sum_{\boldsymbol{\rho}} D_{i+\boldsymbol{\rho},j}^{\bar{X}A}(\tau). \end{aligned} \quad (4.14)$$

We define the transformation

$$D^X(\mathbf{q}, i\nu_m) \equiv \int_0^\beta d\tau e^{i\nu_m \tau} \sum'_{i \in X_1} e^{-i\mathbf{q} \cdot \mathbf{R}_{ij}} D_{ij}^{XA}(\tau), \quad (4.15)$$

where $\nu_m \equiv 2m\pi T$ is the Matsubara frequency with $m = 0, \pm 1, \pm 2, \dots$.

From

$$\int_0^\beta d\tau e^{i(\nu_m - \nu_{m'})\tau} = \beta \delta_{mm'}, \quad (4.16)$$

$$\sum_{\nu_m} e^{i\nu_m(\tau - \tau')} = 2\pi \delta(\tau - \tau'), \quad (4.17)$$

$$\sum'_{i \in X_1} e^{i(\mathbf{q} - \mathbf{q}') \cdot \mathbf{R}_i} = \frac{N}{2} \delta_{\mathbf{q}\mathbf{q}'}, \quad (4.18)$$

$$\sum'_{\mathbf{q}} e^{i\mathbf{q} \cdot (\mathbf{R}_i - \mathbf{R}_j)} = \frac{N}{2} \delta_{ii'}, \quad (4.19)$$

the inverse transformation is

$$D_{ij}^{XA}(\tau) = \frac{1}{2\pi} \sum_{\nu_m} e^{-i\nu_m \tau} \frac{2}{N} \sum'_{\mathbf{q}} e^{i\mathbf{q} \cdot \mathbf{R}_{ij}} D^X(\mathbf{q}, i\nu_m). \quad (4.20)$$

Therefore, we obtain

$$\begin{aligned} & (-1)^X i\nu_m D^X(\mathbf{q}, i\nu_m) \\ &= 2m\delta_{XA} + \alpha_1 D^X(\mathbf{q}, i\nu_m) + \alpha_{10} \gamma_{\mathbf{q}} D^{\bar{X}}(\mathbf{q}, i\nu_m), \end{aligned} \quad (4.21)$$

where

$$\gamma_{\mathbf{q}} \equiv \frac{1}{z_1} \sum_{\rho} e^{i\mathbf{q} \cdot \rho}. \quad (4.22)$$

By solving Eq. (4.21), we find

$$D^A(\mathbf{q}, i\nu_m) = \frac{-2m(i\nu_m + \alpha_1)}{\nu_m^2 + \omega_{\mathbf{q}}^2}, \quad (4.23)$$

$$D^B(\mathbf{q}, i\nu_m) = \frac{2m\alpha_{10}\gamma_{\mathbf{q}}}{\nu_m^2 + \omega_{\mathbf{q}}^2}, \quad (4.24)$$

where $\omega_{\mathbf{q}} \equiv \alpha_{10} \sqrt{(1 + \delta_1)^2 - \gamma_{\mathbf{q}}^2}$.

Note the identical equation

$$\langle s_{j \in A}^- s_{i \in X}^+ (t) \rangle = \frac{i}{2\pi} \frac{2}{N} \sum_{\mathbf{q}}' e^{i\mathbf{q} \cdot \mathbf{R}_{ij}} \int_{-\infty}^{\infty} d\omega e^{-i\omega t} \{D^X(\mathbf{q}, \omega + i\eta) - D^X(\mathbf{q}, \omega - i\eta)\} \frac{1}{e^{\beta\omega} - 1}, \quad (4.25)$$

where η is the infinitesimal, i.e., $\eta = +0$. We find

$$\begin{aligned} & D^A(\mathbf{q}, \omega + i\eta) - D^A(\mathbf{q}, \omega - i\eta) \\ &= (-2\pi i) m \{(\alpha_1/\omega_{\mathbf{q}} + 1)\delta(\omega - \omega_{\mathbf{q}}) - (\alpha_1/\omega_{\mathbf{q}} - 1)\delta(\omega + \omega_{\mathbf{q}})\}, \end{aligned} \quad (4.26)$$

$$\begin{aligned} & D^B(\mathbf{q}, \omega + i\eta) - D^B(\mathbf{q}, \omega - i\eta) \\ &= -(-2\pi i) \frac{m\alpha_{10}\gamma_{\mathbf{q}}}{\omega_{\mathbf{q}}} \{\delta(\omega - \omega_{\mathbf{q}}) - \delta(\omega + \omega_{\mathbf{q}})\}, \end{aligned} \quad (4.27)$$

because

$$\lim_{\eta \rightarrow +0} \left(\frac{1}{x + i\eta} - \frac{1}{x - i\eta} \right) = -2\pi i \delta(x). \quad (4.28)$$

Thus, we obtain

$$\begin{aligned} & \langle s_{j \in A}^- s_{i \in A}^+ (t) \rangle \\ &= m \frac{2}{N} \sum_{\mathbf{q}}' e^{i\mathbf{q} \cdot \mathbf{R}_{ij}} \left\{ \frac{(\alpha_1/\omega_{\mathbf{q}} + 1)e^{-i\omega_{\mathbf{q}} t}}{e^{\beta\omega_{\mathbf{q}}} - 1} - \frac{(\alpha_1/\omega_{\mathbf{q}} - 1)e^{i\omega_{\mathbf{q}} t}}{e^{-\beta\omega_{\mathbf{q}}} - 1} \right\}, \end{aligned} \quad (4.29)$$

$$\langle s_{j \in A}^- s_{i \in B}^+ (t) \rangle = -m\alpha_{10} \frac{2}{N} \sum_{\mathbf{q}}' e^{i\mathbf{q} \cdot \mathbf{R}_{ij}} \frac{\gamma_{\mathbf{q}}}{\omega_{\mathbf{q}}} \left(\frac{e^{i\omega_{\mathbf{q}} t}}{e^{\beta\omega_{\mathbf{q}}} - 1} - \frac{e^{-i\omega_{\mathbf{q}} t}}{e^{-\beta\omega_{\mathbf{q}}} - 1} \right). \quad (4.30)$$

When $i = j = l \in A$ and $t = 0$, Eq. (4.29) becomes

$$\langle s_{l \in A}^- s_{l \in A}^+ \rangle = m \frac{2}{N} \sum_{\mathbf{q}}' \left\{ \frac{\alpha_1}{\omega_{\mathbf{q}}} \coth \left(\frac{\beta \omega_{\mathbf{q}}}{2} \right) - 1 \right\}. \quad (4.31)$$

When $i = l \in A$, $j = m \in B$ and $t = 0$, Eq. (4.30) becomes

$$\langle s_{l \in A}^- s_{m \in B}^+ \rangle = -m \alpha_{10} \frac{2}{N} \sum_{\mathbf{q}}' \frac{\gamma_{\mathbf{q}}}{\omega_{\mathbf{q}}} \coth \left(\frac{\beta \omega_{\mathbf{q}}}{2} \right) e^{i\mathbf{q} \cdot \mathbf{R}_{ml}}. \quad (4.32)$$

By using Eq. (4.31) and the relation $\langle s_{l \in A}^- s_{l \in A}^+ \rangle = 1/2 - m$ for $s = 1/2$, we obtain the self-consistent equation is

$$\frac{1}{2m} = \frac{2}{N} \sum_{\mathbf{q}}' \frac{1 + \delta_1}{\sqrt{(1 + \delta_1)^2 - \gamma_{\mathbf{q}}^2}} \coth \left(\frac{z_1 J_1 m}{2T} \sqrt{(1 + \delta_1)^2 - \gamma_{\mathbf{q}}^2} \right). \quad (4.33)$$

The critical temperature at which m and M vanish is obtained as

$$T_c = \frac{1 + \delta_{1c}}{f_n(\delta_{1c})} T_{1c}^{\text{MF}}, \quad (4.34)$$

where

$$f_n(\delta_1) \equiv \frac{2}{N} \sum_{\mathbf{q}}' \frac{1}{1 - \{\gamma_{\mathbf{q}} / (1 + \delta_1)\}^2}, \quad (4.35)$$

$$\delta_{1c} \equiv \lim_{T \rightarrow T_c} \delta_1 = \lim_{T \rightarrow T_c} \frac{z_{12} J_{12} M}{z_1 J_1 m} = \frac{(z_{12} J_{12})^2}{z_1 J_1 z_2 J_2} \frac{T_{c2}^{\text{MF}}}{T_c - T_{c2}^{\text{MF}}}. \quad (4.36)$$

$T_{c\ell}^{\text{MF}}$ is the critical temperature of subsystem ℓ in the mean-field approximation, which is expressed as

$$T_{c\ell}^{\text{MF}} \equiv \frac{z_{\ell} J_{\ell} S_{\ell} (S_{\ell} + 1)}{3}. \quad (4.37)$$

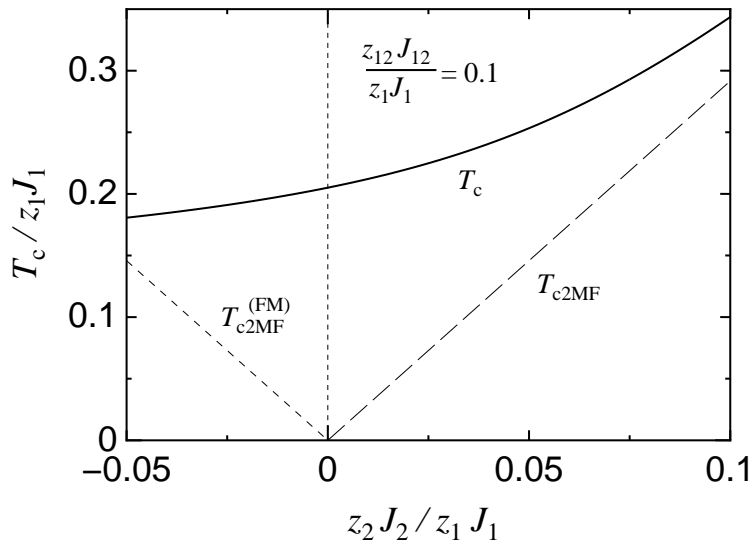


Figure 4.1: \mathcal{J}_2 dependence of the critical temperature T_c . $\mathcal{J}_{12} = \mathcal{J}_1/10$ is fixed. The solid, dashed, and short-dashed curves indicate T_c , T_{c2MF} , and $T_{c2MF}^{(FM)}$, respectively, where T_{c2MF} and $T_{c2MF}^{(FM)}$ are the transition temperatures in subsystem 2 based on the mean-field approximation for $\mathcal{J}_2 > 0$ and $\mathcal{J}_2 < 0$, respectively. This figure is presented in Ref. [37].

In particular, $T_{c1}^{MF} = z_1 J_1/4$ for $s = 1/2$. In Eq. (4.36), we have used

$$\lim_{T \rightarrow T_c} \frac{M}{m} = \frac{z_{12} J_{12}}{z_2 J_2} \frac{T_{c2}^{MF}}{T_c - T_{c2}^{MF}}, \quad (4.38)$$

which is obtained from the self-consistent equation shown in Eq. (4.8).

4.2 Results

We calculate the sublattice magnetizations m and M and the critical temperature T_c from the self-consistent equations of Eqs. (4.8) and (4.33).

Figure 4.1 shows \mathcal{J}_2 dependence of the critical temperature T_c , where $\mathcal{J}_{12} = \mathcal{J}_1/10$ is fixed. We find that T_c takes the value near $T_{c1MF} = \mathcal{J}_1/4$ even when \mathcal{J}_2 is ferromagnetic, i.e., $\mathcal{J}_2 \leq 0$.

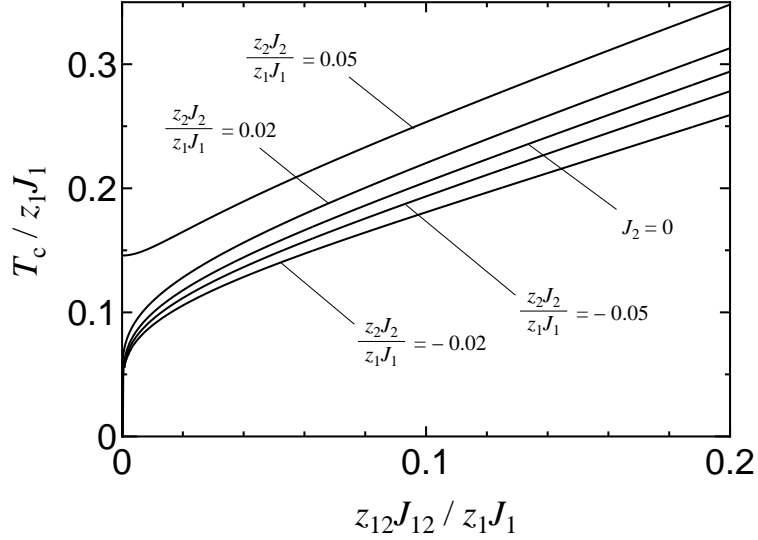


Figure 4.2: \mathcal{J}_{12} dependence of the critical temperature T_c for $\mathcal{J}_2/\mathcal{J}_1 = 0, \pm 0.02, \text{ and } \pm 0.05$. This figure is presented in Ref. [37].

Figure 4.2 shows \mathcal{J}_{12} dependence of the critical temperature T_c . We find the rapid increase of T_c near $\mathcal{J}_{12} = 0$ as \mathcal{J}_{12} increases. At $\mathcal{J}_{12} = 0$, we find that $T_c = T_{c2MF}$ for $\mathcal{J}_2 > 0$, because the independent subsystem 1 does not exhibit the phase transition at any finite temperature, in accordance with Mermin–Wagner theorem, and the critical temperature of the independent subsystem 2 is T_{c2MF} .

Figure 4.3 shows \mathcal{J}_1 dependence of the critical temperature T_c . When we compare the results of $\mathcal{J}_2 = 0$ and 0.3 K for $\mathcal{J}_{12} = 5$ K, we find that the difference of T_c is very small. Hence, for simplicity, we examine the critical temperature for $\mathcal{J}_2 = 0$. Since from the estimation of the overlap integrals by Mori et al. [12], $\mathcal{J}_{12} \approx \mathcal{J}_1/10$, we obtain $\mathcal{J}_1 = 40$ K and $\mathcal{J}_{12} = 4$ K, which give the experimental critical temperature $T_c \approx 8.3$ K.

For $\mathcal{J}_1 = 0$, the present theory is reduced to the mean-field theory because only the terms of J_1 take into account the fluctuation by Tyablikov approximation. In Fig. 4.3, the solid lines indicate the finite value $T_c = \sqrt{105} \mathcal{J}_{12}/12$

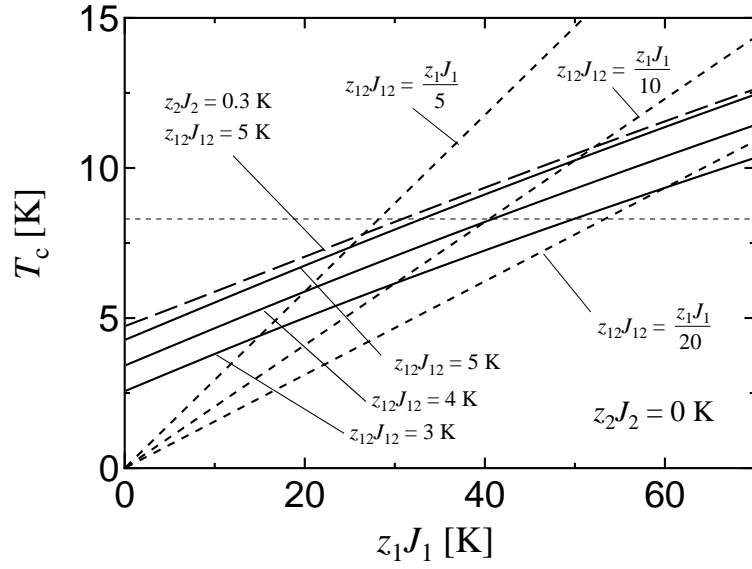


Figure 4.3: \mathcal{J}_1 dependence of the critical temperature T_c . $\mathcal{J}_2 = 0$ is fixed except for the dashed line. The solid curves are the result for $\mathcal{J}_{12} = 3, 4,$ and 5 K. The short-dashed curves are the result for $\mathcal{J}_{12}/\mathcal{J}_1 = 1/5, 1/10,$ and $1/20$. The dashed curve is the result for $\mathcal{J}_{12} = 5$ K and $\mathcal{J}_2 = 0.3$ K. The thin dotted line is the experimental values of the critical temperature in λ -(BETS) $_2$ FeCl $_4$, $T_c \approx 8.3$ K. This figure is presented in Ref. [37].

at $\mathcal{J}_1 = 0$. The error of the mean-field theory is large for $z_{12} = 1$ and $z_1 J_1, z_2 J_2 \ll J_{12}$. In this limit of $z_{12} = 1$ and $J_1 = J_2 = 0$, the system is just an aggregation of a number of uncoupled two-spin systems, which does not exhibit the antiferromagnetic order at any finite temperature. This discrepancy is due to the fact that the mean-field approximation ignores the fluctuation due to the small number of degrees of freedom. However, the present theory is applicable to λ -(BETS)₂FeCl₄, since $\mathcal{J}_1 \gg \mathcal{J}_{12}$ in this compound.

We calculate the sublattice magnetizations m and M . According to Mermin–Wagner theorem, in the isotropic Heisenberg model, the sublattice magnetizations are not finite at any finite temperature. Thus, in this model $m = M = 0$ when $J_2 = J_{12} = 0$ even for large J_1 . The present theory reproduces this behavior.

The results for $\mathcal{J}_{12} \neq 0$ are obtained by numerical calculations. Figure 4.4 shows the temperature dependence of the sublattice magnetizations, where $\mathcal{J}_2 \neq 0$ is fixed. The behavior of M is not similar to that of the simple Heisenberg model. For $\mathcal{J}_{12} = \mathcal{J}_1/100$, M is less than $1/5$ at T above $0.5 \times T_c$, increases rapidly as T decreases below $0.25 \times T_c$, and reaches $S = 5/2$ at $T = 0$, where $T_c \approx \mathcal{J}_1/10$ is approximately equal to $0.4 \times T_{c1MF}$. The temperature dependence of m is different from that of M and similar to that of the simple Heisenberg model.

Figure 4.5 shows the temperature dependence of the sublattice magnetizations, where J_2 is small so that $|J_2/\mathcal{J}_1| \lesssim 1/100$, and $\mathcal{J}_{12}/\mathcal{J}_1 = 1/100$ is fixed. For $J_2 \geq 0$, M increases rapidly near T_{c2MF} as the temperature decreases, and reaches $S = 5/2$ at $T = 0$. For $J_2 < 0$, M does not saturate to $S = 5/2$ even at $T = 0$ with the same magnitude of T_c . Thus, even for small finite \mathcal{J}_{12} , the system exhibits antiferromagnetic order.

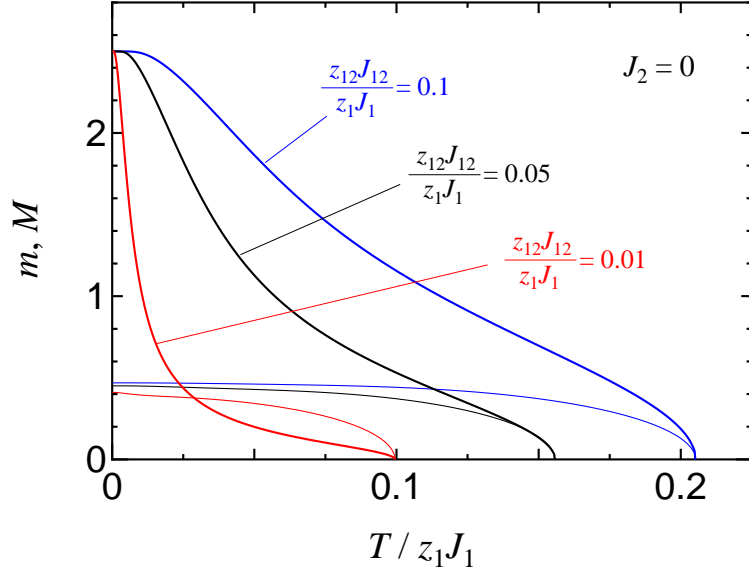


Figure 4.4: Temperature dependence of the sublattice magnetizations m and M for $\mathcal{J}_2 = 0$. The red, black, and blue curves are the results of $\mathcal{J}_2/\mathcal{J}_1 = 0.01$, 0.05, and 0.1, respectively. The thin and thick curves indicate m and M , respectively. This figure is presented in Ref. [37].

4.3 Summary of the chapter

In this chapter, we examined the coupled Heisenberg model, where we assumed the isotropic and anisotropic exchange interactions between π spins and between 3d spins, respectively. To take into account the fluctuation of π spins, we applied Tyablikov approximation to π spins, whereas we adopted the mean-field approximation for 3d spins. It was found that the antiferromagnetic long-range order is stabilized by even weak interactions between the subsystems, regardless of the existence of interactions between 3d spins.

The stabilization mechanism is explained as follows: Solely in the π -spin subsystem, the long-range order is not stabilized because of the low dimensionality. Through the exchange fields, the short-range order of the π spins induces that of the 3d spins. Since the 3d spins are large and anisotropic,

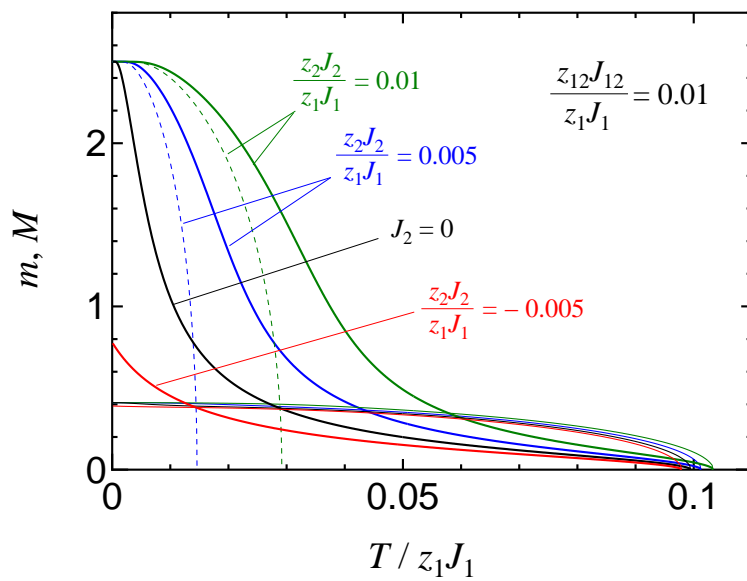


Figure 4.5: Temperature dependence of the sublattice magnetizations m and M . $\mathcal{J}_{12}/\mathcal{J}_1 = 0.01$ is fixed. The red, black, blue, and green curves are the results of $\mathcal{J}_2/\mathcal{J}_1 = -0.005, 0, 0.005,$ and 0.01 , respectively. The thin and thick curves show m and M , respectively. The thin dotted curves show M for $J_{12} = 0$. For $J_{12} = 0$, $m = 0$ at any T in accordance with the Mermin–Wagner theorem. This figure is presented in Ref. [37].

they create the anisotropic exchange field on the π spins. Hence, the fluctuations of the π spins are suppressed, resulting in the long-range order at finite temperatures.

This mechanism becomes efficient because of the marginality of the π -spin system with respect to the phase transition. The long-range order of two-dimensional system is marginally suppressed by the fluctuation. Below the temperatures on the order of J_1 , the correlation length of π -spins increases, which results in large block spins. Hence, even small J_{12} significantly suppresses the fluctuation and stabilizes the long-range order. For instance, $\mathcal{J}_{12} \approx 0.01 \times \mathcal{J}_1$ gives T_c on the order of $0.1 \times \mathcal{J}_1$, which is comparable with $T_{\text{c1MF}} = 0.25 \times \mathcal{J}_1$. Even extremely small J_{12} gives sufficiently large T_c that can be observed experimentally. For example, $J_2 \sim 1 \times 10^{-13} J_1$ gives $T_c \sim 0.05 \times J_1$.

For $\mathcal{J}_{12} = 0.1 \times \mathcal{J}_1$, we obtain $T_c \approx 0.2 \times \mathcal{J}_1$, which is comparable with T_{c1MF} . The experimental result $T_c = 8.3 \text{ K}$ is reproduced by the parameters $\mathcal{J}_1 \sim 40 \text{ K}$, $\mathcal{J}_{12} \sim 4 \text{ K}$, and $\mathcal{J}_2 \sim 0.3 \text{ K}$ for the square lattice, which give $J_1 \sim 10 \text{ K}$ and $J_2 \sim 0.08 \text{ K}$. For the triangular lattice, because of the frustration, J_1 and J_2 need to be larger than these values, which is more similar to the real material. However, the present order estimation is consistent with the results of the low-temperature specific heat obtained in Chap. 3.

We adopt the localized spin model for π -electron system in the insulating phase below T_c . This assumption is inappropriate near T_c even in the insulating phase because of the precursor to the metallic phase. Since π spins begin to spread over more than one lattice sites, the lengths of the localized spin moments shrink and may become less than $s = 1/2$. The real m decreases more rapidly than the theoretical estimation. Thus, the theoretical T_c based on this model would be underestimated. The antiferromagnetic order plays

an important role in the localization of π electrons. Thus, the localized spin model is inappropriate when m is sufficiently small. It is difficult to calculate the threshold of m taking into account the correlation effect. As shown in Figs. 4.4 and 4.5, below T_c , m remains large in a wide temperature region with a narrow region near T_c excluded. This picture is also supported by the electric resistivity measurement [6], which implies that the metal-insulator transition occurs in a temperature region between about 8 and 9.5 K. Therefore, this effect does not change the present qualitative and semiquantitative results.

The increase of M is slow at high temperatures, and rapid near T_{c2MF} as the temperature decreases as shown in Figs. 4.4 and 4.5. M becomes $S = 1/2$ at $T = 0$. This behavior implies that 3d spins passively follow the antiferromagnetic order of the π spins. This result is consistent with that of the analysis of the specific heat. Therefore, the 3d spins exhibit the passive order and induce the antiferromagnetic long-range order of the π spins.

The theory presented in this chapter does not exclude the other possibilities of the stabilization mechanisms such as the interlayer interactions, and does not explain the metal-insulator transition. These problems are left for the future study.

In conclusion of this chapter, we explained the stabilization mechanism of the low-dimensional isotropic quantum spin system by the additional anisotropic semiclassical spins. In this mechanism, even weak interactions between two subsystems induce high critical temperature comparable with that of the mean-field theory. The antiferromagnetic order of the 3d spins is passive in accordance with the observation on the specific heat [17]. In the absence of the 3d spins, the π -electron system does not exhibit antiferromagnetic long-range order. This behavior is consistent with the absence of the

antiferromagnetic long-range order in the sister compound λ -(BETS)₂GaCl₄.

Chapter 5

Conclusion

In Chap. 3, we examined the low-temperature properties of λ -(BETS)₂FeCl₄ on the basis of the mean-field approximation. We derived the self-consistent equations of the sublattice magnetizations and the expressions for the specific heat and spin susceptibility. In the analysis of the specific heat, we examined three models in low, intermediate, and high temperature regions, and estimated the values of the model parameters as $\Delta_d \approx 5.61$ K, $z_{12}J_{12} \approx 9.3$ K, $z_2J_2 \approx 3.84$ K, and 60 K $\lesssim z_1J_1 \lesssim 80$ K, using the least-squares method. In the analysis of the spin susceptibility, we examined the four cases of the isotropic or anisotropic limits, and estimated the angle θ between the easy axis and c -axis as $\theta \approx 27^\circ$. It was found that the anisotropy originates from J_{12}^μ rather than from J_2^μ for the experimental value $\theta \approx 30^\circ$. We consistently reproduced the specific heat and spin susceptibility, using these estimated parameters. We confirmed $z_1J_1 \gg z_{12}J_{12} \gg z_2J_2$.

In Chap. 4, we examined the stabilization mechanism of the antiferromagnetic long-range order. We adopted the Tyablikov and mean-field approximations for the π and 3d spins, respectively. It was found that the critical temperature is of the order of $T_{\text{c1MF}} \approx J_1/4$ even for the weak inter-

action between the subsystems regardless of the existence of the interaction between the 3d spins. It was found that the parameters $z_1 J_1 = 40 \text{ K}$ and $z_{12} J_{12} = 4 \text{ K}$ reproduce the experimental critical temperature $T_c \approx 8.3 \text{ K}$. The temperature dependence of the sublattice magnetizations implies that the 3d spins passively follow the antiferromagnetic long-range order formed in the π -spin system. The antiferromagnetic long-range order of the low-dimensional isotropic quantum-spin main system is stabilized by the additional anisotropy due to the semiclassical spin subsystem. Even when the inter-subsystem coupling is extremely weak, the resultant T_c can be comparable to the mean-field transition temperature of the isolated main system.

Reference

- [1] A. Kobayashi, T. Udagawa, H. Tomita, T. Naito, and H. Kobayashi, *Chem. Lett.* **22**, 2179 (1993).
- [2] F. Goze, V. Laukhin, L. Brossard, A. Audouard, J. Ulmet, S. Askenazy, T. Naito, H. Kobayashi, A. Kobayashi, M. Tokumoto, and P. Cassoux, *Synth. Met.* **71**, 1901 (1995).
- [3] H. Kobayashi, H. Tomita, T. Naito, A. Kobayashi, F. Sakai, T. Watanabe, and P. Cassoux, *J. Am. Chem. Soc.* **118**, 368 (1996).
- [4] H. Akutsu, E. Arai, H. Kobayashi, H. Tanaka, A. Kobayashi, and P. Cassoux, *J. Am. Chem. Soc.* **119**, 12681 (1997).
- [5] H. Kobayashi, A. Sato, E. Arai, H. Akutsu, A. Kobayashi, and P. Cassoux, *J. Am. Chem. Soc.* **119**, 12392 (1997).
- [6] A. Sato, E. Ojima, H. Akutsu, H. Kobayashi, A. Kobayashi, and P. Cassoux, *Chem. Lett.* **27**, 673 (1998).
- [7] L. Brossard, R. Clerac, C. Coulon, M. Tokumoto, T. Ziman, D. Petrov, V. Laukhin, M. Naughton, A. Audouard, F. Goze, A. Kobayashi, H. Kobayashi, and P. Cassoux, *Eur. Phys. J. B* **1**, 439 (1998).

- [8] H. Kobayashi, A. Kobayashi, and P. Cassoux, *Chem. Soc. Rev.* **29**, 325 (2000).
- [9] S. Uji, H. Shinagawa, C. Terakura, T. Terashima, T. Yakabe, Y. Terai, M. Tokumoto, A. Kobayashi, H. Tanaka, and H. Kobayashi, *Phys. Rev. B* **64**, 024531 (2001).
- [10] S. Uji, H. Shinagawa, T. Terashima, T. Yakabe, Y. Terai, M. Tokumoto, A. Kobayashi, H. Tanaka, and H. Kobayashi, *Nature(London)* **410**, 908 (2001).
- [11] T. Sasaki, H. Uozaki, S. Endo, and N. Toyota, *Synth. Met.* **120**, 759 (2001).
- [12] T. Mori and M. Katsuhara, *J. Phys. Soc. Jpn.* **71**, 826 (2002).
- [13] S. Uji, C. Terakura, T. Terashima, T. Yakabe, Y. Terai, M. Tokumoto, A. Kobayashi, F. Sakai, H. Tanaka, and H. Kobayashi, *Phys. Rev. B* **65**, 113101 (2002).
- [14] M. Watanabe, S. Komiyama, R. Kiyonagi, Y. Noda, E. Negishi, and N. Toyota, *J. Phys. Soc. Jpn.* **72**, 452 (2003).
- [15] S. Komiyama, M. Watanabe, Y. Noda, E. Negishi, and N. Toyota, *J. Phys. Soc. Jpn.* **73**, 2385 (2004).
- [16] S. Uji and J. S. Brooks, *J. Phys. Soc. Jpn.* **75**, 051014 (2006).
- [17] H. Akiba, S. Nakano, Y. Nishio, K. Kajita, B. Zhou, A. Kobayashi, and H. Kobayashi, *J. Phys. Soc. Jpn.* **78**, 033601 (2009).
- [18] H. Akiba, K. Nobori, K. Shimada, Y. Nishio, K. Kajita, B. Zhou, A. Kobayashi, and H. Kobayashi, *J. Phys. Soc. Jpn.* **80**, 063601 (2011).

- [19] H. Akiba, H. Sugawara, K. Nobori, K. Shimada, N. Tajima, Y. Nishio, K. Kajita, B. Zhou, A. Kobayashi, and H. Kobayashi, *J. Phys. Soc. Jpn.* **81**, 053601 (2012).
- [20] H. Akiba, K. Shimada, N. Tajima, K. Kajita, and Y. Nishio, *Crystals* **2**, 984 (2012).
- [21] Y. Oshima, H. Nojiri, S. Uji, J. S. Brooks, T. Tokumoto, H.-B. Cui, R. Kato, A. Kobayashi, and H. Kobayashi, *Phys. Rev. B* **86**, 024525 (2012).
- [22] K. Shimada, H. Akiba, N. Tajima, K. Kajita, Y. Nishio, R. Kato, A. Kobayashi, and H. Kobayashi, *JPS Conf. Proc.* **1**, 012110 (2014).
- [23] M. Tokumoto, T. Naito, H. Kobayashi, A. Kobayashi, V. Laukhin, L. Brossard, and P. Cassoux, *Synth. Met.* **86**, 2161 (1997).
- [24] L. Balicas, J. S. Brooks, K. Storr, S. Uji, M. Tokumoto, H. Tanaka, H. Kobayashi, A. Kobayashi, V. Barzykin, and L. P. Gor'kov, *Phys. Rev. Lett.* **87**, 067002 (2001).
- [25] M. Houzet, A. Buzdin, L. Bulaevskii, and M. Maley, *Phys. Rev. Lett.* **88**, 227001 (2002).
- [26] H. Shimahara, *J. Phys. Soc. Jpn.* **71**, 1644 (2002).
- [27] V. Jaccarino and M. Peter, *Phys. Rev. Lett.* **9**, 290 (1962).
- [28] H. Fujiwara, E. Fujiwara, Y. Nakazawa, B. Z. Narymbetov, K. Kato, H. Kobayashi, A. Kobayashi, M. Tokumoto, and P. Cassoux, *J. Am. Chem. Soc.* **123**, 306 (2001).

- [29] T. Otsuka, A. Kobayashi, Y. Miyamoto, J. Kiuchi, S. Nakamura, N. Wada, E. Fujiwara, H. Fujiwara, and H. Kobayashi, *J. Solid State Chem.* **159**, 407 (2001).
- [30] H. Kobayashi, H. Tanaka, E. Ojima, H. Fujiwara, Y. Nakazawa, T. Otsuka, A. Kobayashi, M. Tokumoto, and P. Cassoux, *Synth. Met.* **120**, 663 (2001).
- [31] T. Konoike, S. Uji, T. Terashima, M. Nishimura, S. Yasuzuka, K. Enomoto, H. Fujiwara, B. Zhang, and H. Kobayashi, *Phys. Rev. B* **70**, 094514 (2004).
- [32] Y. Suginishi and H. Shimahara, *Phys. Rev. B* **74**, 024518 (2006).
- [33] J. C. Waerenborgh, S. Rabaça, M. Almeida, E. B. Lopes, A. Kobayashi, B. Zhou, and J. S. Brooks, *Phys. Rev. B* **81**, 060413(R) (2010).
- [34] H. Kobayashi, T. Udagawa, H. Tomita, K. Bun, T. Naito, and A. Kobayashi, *Chem. Lett.* **22**, 1559 (1993).
- [35] N. D. Mermin and H. Wagner, *Phys. Rev. Lett.* **17**, 1133 (1966).
- [36] M. Tokumoto, H. Tanaka, T. Otsuka, H. Kobayashi, and A. Kobayashi, *Polyhedron* **24**, 2793 (2005).
- [37] H. Shimahara and K. Ito, *J. Phys. Soc. Jpn.* **83**, 114702 (2014).
- [38] C. Hotta and H. Fukuyama, *J. Phys. Soc. Jpn.* **69**, 2577 (2000).
- [39] O. Cépas, R. H. McKenzie, and J. Merino, *Phys. Rev. B* **65**, 100502 (2002).
- [40] S. V. Tyablikov, *Ukrain. Math. Zh.* **11**, 287 (1959).

- [41] K. Ito and H. Shimahara, J. Phys. Soc. Jpn. **85**, 024704 (2016).
- [42] K. Hiraki, H. Mayaffre, M. Horvati, C. Berthier, S. Uji, T. Yamaguchi, H. Tanaka, A. Kobayashi, H. Kobayashi, and T. Takahashi, J. Phys. Soc. Jpn. **76**, 124708 (2007).

公表論文

- (1) Mean Field Theory of a Coupled Heisenberg Model and Its Application to an Organic Antiferromagnet with Magnetic Anions
Kazuhiro Ito and Hiroshi Shimahara
Journal of the Physical Society of Japan, **85**, 024704-1 - 024704-7 (2016).
- (2) Stabilization of Long-Range Order by Additional Anisotropic Spins in Two-Dimensional Isotropic Heisenberg Antiferromagnets —A Possible Model of an Organic Compound with Magnetic Anions—
Hiroshi Shimahara and Kazuhiro Ito
Journal of the Physical Society of Japan, **83**, 114702-1 - 114702-7 (2014).